HHS Public Access

Author manuscript

J Physiol. Author manuscript; available in PMC 2025 September 01.

Published in final edited form as:

J Physiol. 2024 September ; 602(18): 4387–4407. doi:10.1113/JP284807.

Neutral Sphingomyelinase Regulates Mechano-Transduction in Human Engineered Cardiac Tissues and Mouse Hearts

Daniel G. P. Turner[1], **Willem J. De Lange, Ph.D.**[2], **Yanlong Zhu, Ph.D.**[3,4], **Christopher L. Coe, Ph.D.**[5], **Judith Simcox, Ph.D.**[6], **Ying Ge, Ph.D.**[3,4,7], **Timothy J. Kamp, Ph.D., M.D.**[1], **J. Carter Ralphe, M.D.**[2], **Alexey V. Glukhov, Ph.D.**[1]

[1] –Department of Medicine, Cardiovascular Medicine, University of Wisconsin-Madison, Madison, WI, 53705, USA.

[2] –Department of Pediatrics, Pediatric Cardiology, University of Wisconsin-Madison, Madison, WI, 53705, USA.

[3] –Human Proteomics Program, School of Medicine and Public Health, University of Wisconsin-Madison, Madison, WI, 53705, USA.

[4] –Department of Cell and Regenerative Biology, University of Wisconsin-Madison, Madison, WI, 53705, USA.

[5] –Department of Psychology, University of Wisconsin-Madison, Madison, WI, 53706, USA

[6] –Department of Biochemistry, University of Wisconsin-Madison, Madison, WI, 53705, USA

[7] –Department of Chemistry, University of Wisconsin-Madison, Madison, WI, 53705, USA.

Abstract

Cardiovascular disease is the leading cause of death in the United States and is known to be exacerbated by elevated mechanical stress from hypertension. Caveolae are plasma membrane structures that buffer mechanical stress but have been found to be reduced in pathological conditions associated with chronically stretched myocardium. To explore the physiologic implications of caveolae loss, we utilize human engineered cardiac tissue (ECT) constructs composed of human-induced pluripotent stem cell (hiPSC)-derived cardiomyocytes and hiPSC-derived cardiac fibroblasts, to develop a long-term cyclic stretch protocol that recapitulates the effects of hypertension on caveolae expression, membrane tension, and β-adrenergic response. Leveraging this novel stretch protocol, we identified neutral sphingomyelinases (nSMase) as mechano-regulated mediators of caveolae loss, ceramide production, and blunted β-adrenergic response in this human cardiac model. Specifically, in our ECT model, nSMase inhibition via

[*]**To whom correspondence should be addressed:** Glukhov AV, 8455 WIMR II, 1111 Highland Ave., Madison, Wisconsin 53705, USA. aglukhov@medicine.wisc.edu.

Author Contributions

DT designed the study, collected significant portions of data, analyzed all data, wrote the majority of the manuscript, and generated figures. WD collected and assisted in ECT contraction data analysis and writing. YZ and YG collected and assisted in analysis and writing of mass spectrometry data. CC and JS assisted in human ceramide data collection, analysis, and writing. TK and JR made significant contributions to the design of the study and writing of the manuscript. AG assisted in optical mapping data collection and analysis and made major contributions to the writing of the manuscript, figure generation, and study design.

Competing Interests

The authors declare no conflicts of interest.

GW4869 prevents stretch-induced loss of caveolae-like structures, mitigates nSMase-dependent ceramide production, and maintains ECT contractile kinetic response to isoproterenol. These findings correlate with a blood lipidomic analysis in middle-aged and older adults, which revealed an increase of the circulating levels of ceramides in adults with hypertension. Furthermore, we found that conduction slowing from increased pressure loading in mouse left ventricle is abolished in the context of nSMase-inhibition. Collectively, these findings identify nSMase as a potent drug target for mitigating stretch-induced effects on cardiac function.

Graphical Abstract

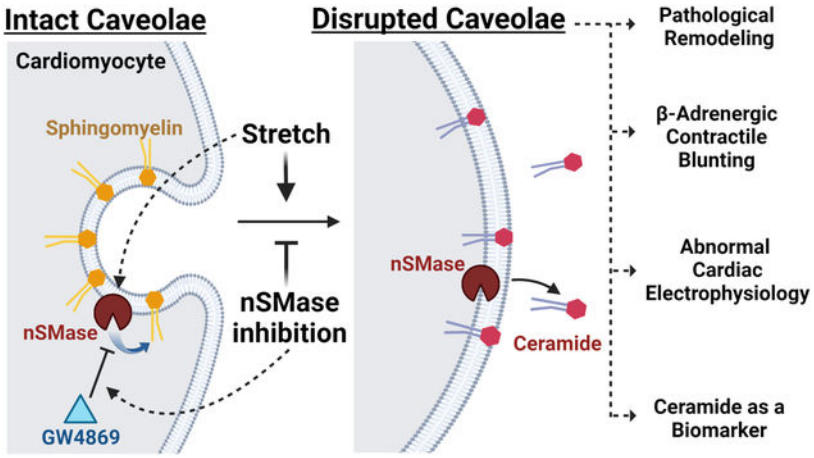

The Journal of Physiology

Cardiomyocyte membranes contain caveolae which buffer mechanical stress and are known to be cardioprotective. Our study found that physical stretch activates neutral sphingomyelinase (nSMase) which converts caveolar sphingomyelin to ceramide leading to disruption of caveolae-like structures in cardiomyocytes. We further linked stretch-induced nSMase activation to electrophysiological changes in myocardium, including decreased ventricular conduction in mouse hearts and blunting of β-adrenergic contractile kinetics and increased ceramide production in engineered human cardiac tissue. These stretch-induced effects were prevented using GW4689, a specific nSMase inhibitor.

Keywords

Caveolae; stretch; neutral sphingomyelinase; hypertension; ceramide; tissue engineering

Introduction

Cardiovascular disease is the leading cause of death worldwide and is often exacerbated by underlying hypertension (Roth *et al.*, 2020). Hypertension results in significant cardiac

remodeling leading to structural and functional changes in the heart, such as increased fibrosis and inflammation (Díez, 2007; Zhang *et al.*, 2020), suppressed contraction, and a blunted response to sympathetic stimulation (Atkins *et al.*, 1995). The possible mechanisms through which hypertension exacerbates cardiovascular disease are complex and reflect the myriad of pathological pathways triggered by high blood pressure, including but not limited to angiotensin II (Jiang *et al.*, 2015), TNF-α (Chen *et al.*, 2010), and TGF-β1 (Zhang *et al.*, 2020). In particular, the molecular mechanisms that underlie stretch-induced changes in ventricular myocardium are not completely understood.

Specialized surface membrane structures known as caveolae, are small (50–100 nm), flask-shaped invaginations of the plasma membrane (Parton & Simons, 2007) and are composed of cholesterol, sphingomyelin, and scaffolding proteins, such as cavins and caveolins (Parton *et al.*, 2018). Caveolae provide a reserve source of “extra” cell membrane and are implicated in cytoprotection and mechano-transduction by buffering mechanical forces and contributing to cell volume regulation (Kozera *et al.*, 2009; Parton & del Pozo, 2013). It has been shown that cardiac caveolae density is decreased in various animal models of cardiovascular disease associated with chronically elevated cardiomyocyte stretch, including hypertension (Egorov *et al.*, 2019), heart failure (Wright *et al.*, 2014), and hypertrophy (Markandeya *et al.*, 2015). However, the mechanisms of caveolae reduction are not well understood.

Neutral sphingomyelinase (nSMase) is a membrane hydrolase enzyme that is involved in sphingolipid metabolism reactions. nSMase activation breaks down sphingomyelin into ceramide species of various sphingosine lengths (depending on sphingomyelin acyl-chain length) and phosphocholine (Wu *et al.*, 2010) and can be inhibited by GW4869 (Wu *et al.*, 2021). In skeletal muscle, caveolin-expressing membrane fractions are enriched for nSMase2 and nSMase3 while nSMase1 does not localize to caveolae (Moylan *et al.*, 2014). In studies performed on non-cardiomyocyte cells, transient mechanical stress induces nSMase activity (Czarny *et al.*, 2003), and prolonged sphingomyelinase activity reduces caveolin protein expression (Makdissy *et al.*, 2018), suggesting nSMase-mediated caveolae disruption. nSMase activation produces ceramide, a potent bioactive lipid that is known to mediate fibrosis (Ji *et al.*, 2017) and can modulate cardiac contractile function (Colligan *et al.*, 2002). Elevated levels of ceramides are also implicated in cardiac hypertrophy and atrial fibrillation (He *et al.*, 2012; Jensen *et al.*, 2020).

Based on these data, we hypothesized that caveolae-localized nSMase (nSMase2 and/or nSMase3) (Moylan *et al.*, 2014) is activated in response to stretch, produces ceramide, decreases caveolae abundance and depresses cardiac conduction velocity that is associated with acute stretch (Pfeiffer *et al.*, 2014). To test this hypothesis, we utilized a validated human engineered cardiac tissue (ECT) model consisting of human-induced pluripotent stem cell (hiPSC)-derived cardiomyocytes and hiPSC-derived cardiac fibroblasts (de Lange *et al.*, 2021). Previously, we demonstrated that these constructs respond to physiological stimuli (stretch and β-adrenergic stimulation), develop a t-tubular system, and demonstrate Ca^{2+}-handling and contractile kinetics that compare favorably with adult myocardium (de Lange *et al.*, 2021). This *in vitro* model is free of the cardiac tissue degeneration normally observed in *ex vivo* cardiac models thus allowing us to evaluate the effect of long-term cardiac stretch without concurrent loss of sample health.

Using our ECT cyclic stretch protocol, we show that stretch reduces abundance of caveolae-like structures, increases membrane tension, and is associated with a blunted contraction kinetic response to isoproterenol. Concurrently, we show that ECT cyclic stretch increases media ceramide levels and hydrogen peroxide, indicating nSMase activation. Specific pharmacological inhibition of nSMase prevented downregulation of caveolae-like structures in the context of elevated mechanical stress and prevented functional changes. We complement these findings with human blood lipidomic data, implicating upregulated nSMase activity in the context of hypertension. Lastly, we demonstrate that acute cardiac stretch in mouse ventricles induces an nSMase-dependent reduction in ventricular electrical conduction and upstroke velocity.

Methods

Ethical Approval

All experimental animal protocols adhered to the *Guidelines for Care and Use of Laboratory Animals* published by the National Institutes of Health (NIH; publication no. 85–23, revised 1996) and were approved by the institutional Animal Care and Use Committee (ACUC) at the University of Wisconsin-Madison (Protocol ID: M005490) with steps taken to minimize pain and suffering. Healthy human hearts that went unused for organ transplant were obtained from the University of Wisconsin Organ Procurement Organization, Madison, WI, USA, as approved by the University of Wisconsin Institutional Review Board (IRB). Blood collection and testing for analysis of ceramide levels in systemic circulation were approved by the Health Sciences IRB at the University of Wisconsin-Madison, as well as by the IRBs at the University of California-Los Angeles and Georgetown University. We confirm that data collection and analysis involving human subjects conformed with the Declaration of Helsinki, except for registration in a database. All authors understand the ethical principles of *The Journal of Physiology* and our study complies with the ethics checklist for research with animal and human subjects.

Stem Cell Culture

DF19-9-11T.H iPSCs, obtained from the WiCell Research Institute (RRID:CVCL_K054), were cultured in StemFlex media (A3349401, Gibco) according to the manufacturer's protocol. Briefly, cryopreserved iPSCs were thawed, added to StemFlex media supplemented with 5 μM Y-27632 (562822, BD Biosciences) and plated onto Growth Factor Reduced Matrigel (354230, Corning) coated six-well dishes (1.5×10^5-3.3×10^5 cells per well ($9.6cm^2$)). hiPSCs were subsequently incubated at 37°C; 5% CO_2 until they were 70%–90% confluent with media changes every 24–48 h with StemFlex prior to passaging. hiPSCs were passaged every 4–6 days using Versene (15040066, Gibco) to dissociate cells according to the manufacturer's protocol, which were then resuspended in StemFlex media, and plated onto Matrigel-coated plates at a 1:6 to 1:12 split ratio.

Cardiomyocyte Stem Cell Differentiation

HiPSCs derived from the DF19-9-11T.H line were differentiated into cardiomyocytes (CMs) using a small molecule-directed (GiWi) protocol as previously described (Zhang *et al.*, 2012; Lian *et al.*, 2013). Briefly, hiPSCs maintained on the StemFlex/Matrigel system were

dissociated into single cells and seeded onto Matrigel-coated six-well plates at 2.0 × 10^6 cells/well in StemFlex media. Cells were cultured for 5 days in StemFlex media with daily media changes. On *day 0*, StemFlex media was replaced with 2.5 mL/well RPMI (11875093) supplemented with B27 without insulin (A1895601, Gibco) supplemented with 10 μM CHIR99021 (2520691, GSK-3 inhibitor, Biogems). Precisely 24 h later (*Day 1*), cell culture media was changed to 3 mL/well RPMI + B27 without insulin. On *day 3*, 48 h later, the media was changed to 3 mL/well RPMI + B27 without insulin supplemented with 5 μM IWP-2 (6866167, Biogems). Precisely 120 h later (*Day 5*), the media was replaced with 3 mL RPMI + B27 without insulin. The media was changed to RPMI + B27 complete supplement (with insulin) (17504044, Gibco) on *Day 7* and cells were maintained in this media until *day 15* with media changes every 24–48 h. On *Day 15*, cells from wells containing ≥50% beating cells by visual inspection were dissociated with 10x TrypLE (A1217701, Thermo Fisher Scientific) according to the manufacturer's protocol. Following resuspension in StemFlex media, cells were replated on Synthemax (3535, Corning) coated six-well plates at 2.0 × 10^6 cells/well. Roughly 48 h after replating, hiPSC-CMs were purified using Lactate media, made with RPMI 1640 with no glucose (11879020, Life Technologies), B27 supplement, and 0.02% (2.66 mM) lactate (L1375, Sigma-Aldrich) for 7 days with media changes every 24–48 h. After selection, CMs were maintained in RPMI with B27 supplement until *Day 30* at which point hiPSC-CMs were dissociated for hiPSC-ECT generation (Fig. 1A).

Stem Cell Cardiac Fibroblast Culture

DF19-9-11T.H hiPSC-cardiac fibroblasts (CFs) were differentiated as previously described and cultured in FibroGRO-LS media (SCMF001, Millipore Sigma) in uncoated six-well culture plates (Corning) with passaging every 4–5 days (Zhang *et al.*, 2019). Media was replaced every 24–48 h. Low passage numbers (<12) were used for hiPSC-ECT generation.

ECT Generation and Cyclic Stretch

Day 30 DF19-9-11T.H hiPSC-CMs were visually inspected and only wells containing ≥95% beating cells were dissociated with 10x TrypLE according to the manufacturer's protocol and counted using a hemocytometer. hiPSC-CMs were subsequently resuspended in fibrin ECT media (60.3% high-glucose DMEM; 20% F12 nutrient supplement; 1 mg/mL gentamicin; 8.75% fetal bovine serum; 6.25% horse serum; 1% HEPES; 1× nonessential amino acid cocktail; 3 mM sodium pyruvate; 0.004% (wt/vol) $NaHCO_3$1 μg/mL insulin; 400 μM tranexamic acid; and 17.5 μg/mL aprotinin) and incubated for at least 1 h on a rotating platform at 37°C to form small and uniform clusters of viable CMs. DF19-9-11T.H CFs were dissociated using 1× TrypLE (12604013, Thermo Fisher Scientific) according to the manufacturer's protocol and counted using a hemocytometer. Following rotational culture, 2 × 10^6 hiPSC-CMs were mixed with 2 × 10^5 hiPSC-CFs in 200 μL fibrin ECT media per hiPSC-ECT, a ratio similar to that previously used in the generation of 3D cardiac constructs (de Lange *et al.*, 2021; De Lange *et al.*, 2023). To this cell mixture, 1.25 mg/mL fibrinogen and 0.5 unit of thrombin were added. This cell-matrix mixture was rapidly mixed and loaded onto a 20×3 mm cylindrical mold of FlexCell™ Tissue Train silicone membrane culture plate (TT4001U) and incubated under pre-programmed vacuum condition for 60 min at 37°C supplied with 5% CO_2 to allow for attachment of the ECT constructs to the nylon

tabs at each end of the Tissue Train well (Fig. 1B). Following polymerization of the fibrin matrix, ECTs were fed with ECT media, carefully separated from the plate surface with a sterile pipette and cultured for 30 days with fibrin ECT media changes every 2–3 days. ECT were stretched days 53–60 (Days 23–30 post-ECT generation) using a FlexCell™ Tissue Train silicone membrane vacuum system (Fig. 1C). The 7-day cyclic stretch protocol was modified from previously published protocols (Prosser *et al.*, 2013; Lu *et al.*, 2021) and set for 0.25 Hz and incrementally increased every 24 h by 3–4% uniaxial elongation, up to 15%. This cyclical and incremental stretch protocol was implemented as nSMase activation is transient under constant mechanical stress (Czarny *et al.*, 2003). During the stretch protocol, all wells were fed every 48 h with ECT medium supplemented with or without GW4869. All unstretched and stretched ECT were fed with 5 mL/well ECT media to maintain a proper volume of cell culture media with concurrent sampling for downstream LC-MS/MS and H_2O_2 analyses.

GW4869 Solubilization

GW4869 (Thermo Fisher Scientific, 501873728), a specific nSMase inhibitor was first diluted to 1.5 mM in dimethyl sulfoxide (DMSO), aliquoted, and stored at −80 °C. Prior to use, aliquots were thawed at 37°C and further solubilized with 5% methano-sulfonic acid at a 1:20 ratio (methanesulfonic acid:DMSO) to make a 1.43 mM GW4869 solution.

Masson's Trichrome Staining and Analysis

Cryo-sectioning of OCT-embedded ECT at 10 μM and Masson's trichrome staining (Cat. No. KTMTR2) was performed by the UW-Madison Translational Research Initiatives in Pathology (TRIP) core facility. Masson's Trichrome staining images were collected using an EVOS cell imaging system at 20x magnification. ECT fibrotic area was evaluated in ImageJ using a custom program calculated as a percentage fibrotic area of total tissue as discussed previously in detail (Glukhov *et al.*, 2012).

ECT Contraction Testing

Contraction traces were measured in day 60 hiPSC-ECT using protocols like those previously described (de Lange *et al.*, 2021). Briefly, each hiPSC-ECT construct was transferred from the culture dish to a model 801B small intact fiber test apparatus (Aurora Scientific) in Krebs–Henseleit buffer [119 mmol/L NaCl, 12 mmol/L glucose, 4.6 mmol/L KCl, 25 mmol/L $NaHCO_3$, 1.2 mmol/L KH_2PO_4, 1.2 mmol/L $MgCl_2$, 1.8 mmol/L $CaCl_2$, gassed with 95% O_2-5% CO_2 (pH 7.4)]. Day 60 hiPSC-ECT constructs were attached with sutures between a model 403A force transducer (Aurora Scientific) and a stationary arm and perfused with 37°C Krebs–Henseleit buffer at a rate of 1 mL/min, and field stimulation initiated at 1 Hz (2.5 ms, 12.5 V). The longitudinal length of each construct was increased stepwise until maximal twitch force was achieved to establish the Frank–Starling relationship. ECT were allowed to equilibrate for 20 min with constant perfusion. Then, twitch force production was measured with at a 1.5 Hz pacing frequency both at baseline and following 5 min preincubation with 1 μM isoproterenol. Data from force measurements was analyzed using IonWizard 6.0 software (IonOptix). Under each condition, contraction transients of 40–60 successive contractions were collected and averaged. These data were

exported to Microsoft Excel and the kinetics of force generation and relaxation were calculated.

Transmission Electron Microscopy (TEM)

Performed by the SMPH Electron Microscopy Facility (UW-Madison), ECT were fixed and prepared for TEM analysis while unstretched to evaluate the maximum membrane mechanical buffering capacity, similarly to previous work (Egorov *et al.*, 2019; de Lange *et al.*, 2021). Briefly, samples were fixed in 2.5% glutaraldehyde, 2.0% paraformaldehyde buffered in 0.1M sodium phosphate buffer for 2 h at room temperature (RT). After osmium post-fixation, dehydration, and embedding, samples were sectioned on a Reichert-Jung Ultracut E ultramicrotome at 80 nm, and post-stained with uranyl acetate and lead citrate. The sectioned samples were viewed at 80 kV on a Philips CM120 transmission electron microscope at 40,000x magnification. Caveolae-like structures were considered 50–100 nm flask-shaped membrane invaginations located within 50 nm from the cell surface. Caveolae-like structures were identified as sub-sarcolemmal (no visible connection to the sarcolemma in the image plane) or visibly integrated into the sarcolemma (flask-like connection to the sarcolemma observed). To quantify the degree of membrane convolution, we defined a membrane convolution index = $(L/L_o - 1)$, where L is the length of membrane contour, and L_o is the length of a straight path connecting the end points of the membrane segment (Fig. 1D).

Mass Spectrometry

ECT media lipids were isolated using a modified bligh-dyer method (Ulmer *et al.*, 2018) from cell culture media (200 μL/sample). The bligh-dyer method was performed as previously described but using a 1:10 sample:solvent ratio during sample incubation with ice-cold methanol and chloroform (1:1) to maximize ceramide extraction. Organic samples were completely dried and reconstituted in 9:1 methanol:toluene. As previously described (Kauhanen *et al.*, 2016), LC-MS/MS experiments were performed using a Bruker Impact II quadrupole time-of-flight (QTOF) mass spectrometer (Bruker Daltonics, Bremen, Germany) coupled to a Waters nanoACQUITY UPLC system (Waters Corporation, Milford, MA, USA) in positive ion mode. A Waters nanoEase M/Z HSS T3 column (100 Å, 1.8 μm, 300 μm × 100 mm) was used for reversed-phase separation. Mobile phase A was 10 mM ammonium acetate in water with 0.1% formic acid, and mobile phase B was 10 mM ammonium acetate in acetonitrile:2-propanol (4:3, v/v) with 0.1% formic acid (Kauhanen *et al.*, 2016). The lipids eluted from the column were infused into the mass spectrometer using an electrospray ion (ESI) source. Lipids were identified by searching the LC–MS/MS data against the databases downloaded from MassBank of North America (MoNA) and internal databases and using Lipid Species Annotation function in MetaboScape 2022b. Detected ceramide values were adjusted with respect to initial ECT media protein concentration evaluated via Nanodrop.

Amplex Red Peroxidase Assay for ROS Production

H_2O_2 production was measured using the supplied Ampled Red Peroxidase Assay kit protocol (Thermo Fisher Scientific, A22188). Briefly, a standard curve generated from the assay kit's supplied 3% H_2O_2 solution was used to validate that H_2O_2 detection in ECT

media samples were within the linear range. Unique ECT media samples were run in triplicate with 50 μL of conditioned ECT media being used for each replicate. Absorbance (560 nm) detected by a Tecan Infinite M200 plate reader was used to determine H_2O_2 production after a 30 min assay incubation at 37°C.

nSMase Activity Assay

Amplex red sphingomyelinase assay kit was used to quantify nSMase activity in ECT according to the manufacturer's protocol (Thermo Fisher Scientific, A12220). Briefly, ECT were lysed and sonicated in CHAPs lysis buffer (150 mM NaCl, 50 mM Tris-HCl, 0.5% CHAPS, 1× protease inhibitor (Bimake). 10 μg of ECT protein (ran in triplicate) with and without nSMase inhibition via GW4869 (20 μM) was used during the assay. Fluorometric measurements were collected after 30 min incubation at 37°C using a Tecan Infinite M200 plate reader with excitation/emission set for 545/590 nm.

MIDUS Participants for Human Ceramide Levels

Ceramide measures were determined from randomly selected adult men and women who were participants in a survey of health and aging among American adults, Midlife in the US (MIDUS). Initially, MIDUS began in 1995–1996 as a survey of adults recruited through random digit dialing and included individuals between 25–74 years of age across the 48 continental states. A second phase was initiated in 2004 when biological samples were obtained from a subset of the original participants who consented to an overnight hospital stay at one of 3 Clinical and Translational Research Centers, either in Madison, WI, Los Angeles, CA, and Washington DC. The lipid data for this analysis were based on 520 adults between 35–86 years of age. A larger panel of biological and clinical measures was determined from the fasted blood samples that were obtained around 0700. As stated previously, sample collection and testing were approved by 3 IRBs (Health Sciences IRB, UW-Madison, as well as by the IRBs at UCLA and Georgetown University. Lipidomic values were generated by mass spectrometry from frozen sera in one batch using (Complex Lipid Panel, Metabolon, Durham, NC). The current analysis focus just on ceramides, but additional information on other lipids can be found in a previous publication (Berkowitz *et al.*, 2022).

Quantitative Reverse Polymerase Chain Reaction

Whole ECTs and human left ventricles were snap frozen in liquid nitrogen post-physiological testing and stored at −80°C. RNA was isolated as previously described (Turner *et al.*, 2022). hiPSC-ECTs were homogenized using TRIzol reagent (Ambion, 15596018) and molecular-grade chloroform was added according to the manufacturer's instructions. After mixing, incubation, and centrifugation, the aqueous phase containing RNA was collected. RNA was further purified using the Qiagen Miniprep kit according to the manufacturer's instructions. RNA was quantified and quality was assessed using a NanoDrop spectrophotometer (Fisher Scientific). 50–100 ng total RNA was reverse transcribed into first-strand cDNA with the iScript Reverse Transcription Supermix for RT-qPCR (Bio-Rad, 170–8890) following manufacturer's protocols. 1 ng of resulting cDNA was used for qPCR analysis. Taqman probes for assayed genes and appropriate controls were arrayed in MicroAmp Optical 96-well Reaction Plates (Applied Biosystems,

4483485), and the PCR performed using the TaqMan Gene Expression Master Mix (Applied Biosystems, 4369016). Real-time monitoring of TaqMan fluorescence was performed on the Bio-Rad RT-qPCR system CFX96. An initial activation step of 2 min at 50°C and 95°C for 10 min was followed by 40 cycles of 15 s of denaturation at 95°C and 60 s of annealing/extension at 60 °C. Data were analyzed in Excel, using a ΔΔCT method as previously described (Turner *et al.*, 2022), with GAPDH used as a housekeeping control gene. TaqMan assay IDs used were GAPDH (Hs02786624_g1), ACTA2 (Hs05005341_m1), COL3A1 (Hs00943809_m1), COL1A2 (Hs01028956_m1), TIMP3 (Hs00165949_m1), MMP2 (Hs01548727_m1), TGF-β1 (Hs00998133_m1), TNF-α (Hs00174128_m1), IL-6 (Hs00174131_m1), SMPD4 (Hs04187047_g1), and SMPD3 (Hs00920354_m1). All TaqMan assays were obtained from Applied Biosystems unless indicated otherwise.

Isolated Mouse Heart Studies

Adult (5 to 7-month-old) male and female C57BL/6 mice (RRID:MGI:2159769) (n=8) were used in the study. Hearts were isolated and Langendorff perfused as described previously (Glukhov *et al.*, 2010). Mice were heparinized and anesthetized, and the heart was removed and placed in oxygenated (95% O_2, 5% CO_2) constant-temperature (37°C), modified Tyrode solution of the following composition (in mmol/L): 128.2 mM NaCl, 4.7 mM KCl, 1.19 NaH_2PO_4, 1.05 mM $MgCl_2$, 1.3 mM $CaCl_2$, 20.0 mM $NaHCO_3$, and 11.1 mM glucose (pH=7.35±0.05). After cannulation, the heart was superfused and retrogradely perfused with warmed (37°C) Tyrode solution under constant aortic pressure of 60 mmHg. The heart was paced at the lateral left ventricular midwall with a silver bipolar electrode coated with Teflon except at the tip. As previously described (Pfeiffer *et al.*, 2014) once isolated and connected to Langendorff perfusion apparatus, a fluid-filled length of polyethylene tubing fitted onto a 20-gauge luer adapter was inserted into the left ventricular cavity via the pulmonary vein and mitral valve. A tie was secured around the opening of the pulmonary vein. The left ventricular cavity tube was connected to a reservoir of warmed and oxygenated perfusate, and left ventricular pressure was controlled by the height of the reservoir relative to the heart.

Optical Mapping of Whole-Mouse Hearts

As previously described (Glukhov *et al.*, 2010), coronary perfused hearts were stained by perfusion with voltage sensitive dye (RH-237, S1109, Thermo Fisher Scientific; 5 μL of 1 mg/ml DMSO, in Tyrode solution) for 10 min. Excitation light (530/540 nm) was generated by a 150-W halogen lamp with an excitation filter (530–40 nm) from a constant-current, low-noise, power supply (MHAB-150W, Moritex USA Inc., CA, USA). The emitted light >660 nm was filtered by a long-pass filter (>660 nm; Thorlabs, NJ) for the action potential signal. The fluorescent light emitted from the preparation was long-pass (>660 nm) filtered using an edge pass filter (Thorlabs, NJ) before reaching the camera. Emitted light was directed towards a MiCAM Ultima-L CMOS camera (SciMedia, CA) with high spatial (100×100 pixels, 60±10 μm/pixel) and temporal (2,000 frames/s) resolution. The acquired fluorescent signal was digitized, amplified, and visualized using custom software (SciMedia, CA). A customized Matlab-based computer program was used to analyze optical signals. Maximum upstroke derivative (dV/dt_{max}) was calculated for each action potential using

the normalized optical signal and its derivatives. Activation maps were constructed during constant 8Hz electrical pacing from activation times, which were determined from the dV/dt_{max}.

Statistical Analysis

For assessing the effect of cyclic stretch on ECT plasma membrane morphology, fibrosis, β-adrenergic stimulation, and stretch-conditioned media, *p* values were calculated with two-way ANOVA with *post-hoc* Bonferroni's multiple comparisons test to test for interactions when comparing multiple groups in cases where the data displayed a normal distribution. If the Shapiro-Wilk test revealed that the data did not have a normal distribution, Kruskal–Wallis ANOVA was used. Statistical significances between normotensive and hypertensive MIDUS participant ceramide data were determined via Welch's student t-tests. Correlations were evaluated using linear regression with significance calculated using an F-test. Statistical analyses were performed in Origin or GraphPad Prism software and *p*-values equal or less than 0.05 were considered statistically significant. All confidence intervals (CI) are 95%.

Results

Chronic Cyclic Stretch alters ECT Plasma Membrane Morphology via nSMase

To determine stretch-induced changes in cardiac myocytes, ECTs were subjected to cyclic stretch for 7 days using a previously published protocol (Lu *et al.*, 2021) for cyclical and incremental stretch modified for elevated mechanical stress. Adjusting for human myocardium, we stretched our ECT at 0.25 Hz and incrementally increased every 24 h by 3–4% elongation, up to 15% length increase over unstretched length, based on Prosser et al. (Prosser *et al.*, 2013). TEM analysis revealed that cyclic stretch reduced abundance of caveolae-like structures by 41%, from 1.87 caveolae/μM (CI 1.53–2.20) in unstretched ECTs to 1.11 caveolae/μM (CI 0.86–1.35) in stretched ECT (p=0.002, two-way ANOVA with *post-hoc* Bonferroni; Fig. 1F). Furthermore, nSMase inhibition via GW4869 (20 μM) applied during the 7-day stretch protocol prevented the effects of cyclic stretch on caveolae-like structure reduction with a 51% increase in stretched ECT treated with GW4869 (1.68 caveolae/μM, CI 1.36–1.98) compared to untreated stretched ECT (1.11 caveolae/μM, CI 0.86–1.35; p=0.045, two-way ANOVA with *post-hoc* Bonferroni). In stretched ECTs, the reduction in caveolae-like structures was accompanied by a 43% decrease in membrane convolution (0.037, CI 0.028–0.046) compared with unstretched ECTs (0.065, CI 0.049–0.081), indicating increased membrane tension (p<0.001, Kruskal-Wallis Test; Fig. 1G) (Wei *et al.*, 2017; Egorov *et al.*, 2019). As anticipated, incubation of GW4869 did not prevent a significant reduction in membrane convolution (p<0.001, Kruskal-Wallis Test) in stretched ECT (0.033, CI 0.027–0.040) vs. unstretched ECT (0.086, CI 0.057–0.115), indicating that despite increased membrane tension, nSMase inhibition still prevents stretch-induced reductions in caveolae-like structures.

Cyclic Stretch Increases Ceramide and ROS in ECT Cell Culture Media

Studies have shown that inflammatory cardiovascular conditions increase ceramide levels in the heart (He *et al.*, 2012) and blood (Jensen *et al.*, 2020); however, the contribution

of nSMase to these increased ceramides is unknown. To explore the potential mechano-activation of nSMase and its role in mediating cardiovascular pathology we utilized LC-MS/MS on ECT cell culture media to determine nSMase activity. LC-MS/MS analysis found that cell culture media collected from cyclically stretched ECT media had a 38% increase of short-chain ceramides (1.00, CI 0.86–1.14) compared to unstretched ECT media (1.38, CI 1.16–1.60; Fig. 2A; p=0.004, two-way ANOVA with *post-hoc* Bonferroni), with no change in long-chain ceramides (Fig. 2B; p=0.560, two-way ANOVA with *post-hoc* Bonferroni). GW4869 treatment prevented short-chain ceramide production between unstretched (1.16, CI 1.06–1.27) and stretched ECT (1.21, CI 1.04–1.37; p=1.00, two-way ANOVA with post-hoc Bonferroni), indicating nSMase as a key mediator of stretch-induced short-chain ceramide production in cardiac tissue. Importantly, we demonstrate that GW4869-treated ECT lysate has nSMase activity (2553, CI 1886–3320) reduced by 32.5% compared to untreated ECT lysate (3644, CI 2680–4609; p=0.005, paired student's t test), suggesting that GW4869 is effective in cardiac tissue (Fig. 2E). Furthermore, our data indicate that GW4869 effectively inhibits nSMase3, as RT-qPCR detected *SMPD4* (encoding nSMase3) but not *SMPD3* (encoding nSMase2) mRNA in ECT or adult human left ventricle and that *SMPD4* is the predominant membrane-associated nSMase in mouse left ventricle (Fig. 2F). RT-qPCR analysis also revealed no changes in *SMPD4* mRNA, when comparing unstretched (0.068, CI 0.042–0.093) and stretched ECT (0.040, CI 0.024–0.11; p=0.846, two-way ANOVA with *post-hoc* Bonferroni correction; Fig. 2D). Protein expression of nSMase3 was unchanged between unstretched and stretched ECT (data not shown). This suggests that nSMase3, not nSMase2, in our ECT is the main nSMase mediator of stretch–induced changes in caveolae-like structures and ceramide production. Overall, these findings support our hypothesis of stretch-induced nSMase activation. Another possible stretch-induced pathogenic factor in myocardium is reactive oxygen species (ROS) (Gao *et al.*, 2021) which have also been shown to play a role in the activation of nSMase via NADPH oxidase (NOX) (Hernandez *et al.*, 2000). While we found that cyclic stretch increases ROS production in ECT media, from 0.33 (CI 0.32–0.34) in unstretched media to 0.36 (CI 0.35–0.37; p<0.001, two-way ANOVA with *post-hoc* Bonferroni correction) in stretched media, it is unaffected by nSMase inhibition with no significant difference between stretched (0.36, CI 0.35–0.37) and stretched+GW4869 (0.37, CI 0.35–0.39; p=1.00, two-way ANOVA with *post-hoc* Bonferroni correction; Fig. 2C). This suggests that nSMase is downstream of NOX2 during mechano-transduction, but additional studies are required to determine if nSMase mechano-activation is NOX2-dependent.

nSMase Inhibition Prevents Chronic Cyclic Stretch Effects on ECT Contraction Kinetics

It has been shown that caveolae play a critical role in the regulation of cyclic adenosine monophosphate (cAMP) signaling and cardiomyocyte response to sympathetic stimulation (Calaghan & White, 2006; Wright *et al.*, 2014). Caveolae loss has been linked to abnormal response to β-adrenergic receptor stimulation (Rybin *et al.*, 2003) and reported for heart failure patients (Böhm *et al.*, 1988). To determine whether the observed stretch-induced reductions in caveolae-like structures modulates ECT response to sympathetic stimulation, we performed contraction testing on unstretched and stretched ECTs. Analysis of ECT twitch amplitude and kinetics before and after treatment with β-adrenergic receptor agonist isoproterenol (1 μM) revealed significant changes in ECT response as demonstrated in

Fig. 3. First, we found that stretched ECT exhibited a significantly blunted response to isoproterenol (p=0.024, Kruskal-Wallis test) as indicated by a 11% decrease of the total contraction time to 100% peak force (CT100) in unstretched ECT (−1.13, CI −2.01 to −0.23) compared to stretched ECT (−0.12, CI −0.53 to 0.29; Fig. 3B). This blunted response was prevented by GW4869 treatment, suggesting an nSMase and caveolae-mediated role. In addition, no significant changes in isoproterenol response were observed in time to 50% and 90% relaxation (RT50 and RT90) between unstretched (−1.34, CI −2.65 to −0.028 and −1.55, CI −2.91 to −0.18, respectively) and stretched ECT (−0.60, CI −1.11 to −0.1 and −0.58, CI −1.06 to −0.1; p=0.735 and 0.436, respectively, two-way ANOVA with *post-hoc* Bonferroni correction; Fig. 3C–D), suggesting that the stretch protocol has a larger effect on excitation-contraction coupling rather than Ca^{2+} reuptake. Looking further, we found that stretched ECT have a 2.0% and 5.5% blunted kinetic response to isoproterenol with respect to contraction times 25–50% and 50–100% (CT25–50 and CT50–100, respectively; p=0.032 and 0.019, respectively, Kruskal-Wallis Test; Fig. 3F–G) but not 0–25% (CT0–25; p=0.663, Kruskal Wallis Test; Fig. 3E). For CT0–25, CT25–50, and CT50–100, unstretched mean ECT relative responses to isoproterenol were −0.48 (CI −0.72 to −0.24), −0.36 (CI −0.51 to −0.20), and −0.28 (CI −0.94 to 0.37), respectively, and stretched ECT responses were −0.23 (CI −0.46 to 0.00), −0.16 (CI −0.23 to −0.08), and 0.27 (CI 0.049 to 0.49). Stretch and nSMase inhibition had no effect on absolute twitch forces, ECT baseline contraction kinetics, or arrhythmogenesis (data not shown) in response to isoproterenol (p=1.00, two-way ANOVA with *post-hoc* Bonferroni correction; Fig. 4). In addition, stretch and GW4869 had no significant effect on sarcomere length (p=1.00, two-way ANOVA with *post-hoc* Bonferroni correction; Fig. 1H) further suggesting the effects of caveolae disassembly on ECT contraction, rather than changes to sarcomere ultrastructure. These findings indicate that our cyclic stretch protocol not only alters ECT plasma membrane morphology but has a significant caveolae- and nSMase-mediated effect on ECT β-adrenergic response.

RT-qPCR of Unstretched and Stretched ECTs of Fibrotic and Inflammatory Pathways

As both chronically elevated stretch (Díez, 2007) and ceramide (Ji *et al.*, 2017) have been linked to the activation of fibrogenesis and inflammatory-associated pathways, we utilized RT-qPCR to evaluate the effect of stretch and nSMase inhibition on our ECTs. We found that stretch and GW4869 have a limited effect on fibrosis. We observed a significant decrease in fibrotic area only between stretched (9.11% fibrosis, CI 7.72–10.50) and stretched+GW4869 ECT (6.52% fibrosis, CI 5.52–7.52; p=0.017, two-way ANOVA with *post-hoc* Bonferroni correction) but no statistically significant change in non-stretched and stretched ECT (p=0.609, two-way ANOVA with *post-hoc* Bonferroni correction), determined by Masson's trichrome staining (Fig. 5A–B). With regard to mRNA expressions, we observed only a significant increase in *ACTA2* between unstretched (1.00, CI 0.66–1.23) and stretched ECT treated with GW4869 (2.16, CI 1.49–2.83; p=0.005, two-way ANOVA with *post-hoc* Bonferroni correction) and unstretched (1.02, CI 0.75–1.29) and stretched ECT both treated with GW4869 (p=0.006, two-way ANOVA with *post-hoc* Bonferroni correction; Fig. 5C). In contrast, qPCR analysis revealed that stretch did not have a significant effect between unstretched and stretched ECT for other fibrosis-related mRNAs such as *COL3A1* (p=0.100, Kruskal-Wallis Test), *COL1A2* (p=0.438, Kruskal-Wallis Test), *TIMP3* (p=0.474, Kruskal-Wallis Test), *MMP2* (p=1.00, two-way ANOVA with *post-hoc* Bonferroni correction), and

TGF-β1 (p=0.603, Kruskal-Wallis Test; Fig. 5D–H). Lastly, mRNAs for the inflammatory cytokines *TNF-α* and *IL-6* were not detected (data not shown).

Effect of Hypertension on Human Circulating Ceramide Levels in Humans

Publicly available blood lipidomic values from the MIDUS survey of health in the US were evaluated to determine if hypertension was similarly correlated to ceramide levels among middle-aged and older American adults (https://www.midus.wisc.edu/). Serum lipidomic data were acquired from ~120 hypertensive and ~420 normotensive adult participants. To identify significant differences in distinct subgroups, individuals were categorized by sex and age (above or below the age of 50). We found that ceramide 18:0 was increased by 22% and 17% in hypertensive males (0.111 μM, CI 0.096–0.126 vs. 0.090 μM, CI 0.083–0.098) and females (0.113 μM, CI 0.104–0.121 vs. 0.0904 μM, CI 0.088–0.100) over the age of 50 (p=0.013 and p<0.001, respectively, Welch's t test), respectively, and ceramide 24:1 was increased by 19% in men over 50 (0.76 μM, CI 0.65–0.87 vs. 0.64 μM, CI 0.60–0.68; p=0.039, Welch's t test; Fig. 6). In men under 50, no ceramides were elevated in hypertensive individuals while ceramides 16:0 and 20:0 were higher by 8% (0.287 μM, CI 0.270–0.304 vs. 0.266 μM, CI 0.256–0.276) and 16% (0.085 μM, CI 0.076–0.094 vs. 0.073 μM, CI 0.067–0.079), respectively, in hypertensive women under 50 years of age (p=0.040 and 0.028, respectively, Welch's t test; Fig. 7A). Interestingly, ceramides 16:0, 24:0, and 24:1 were elevated by 6% (0.282 μM, CI 0.269–0.295 vs. 0.266 μM, CI 0.256–0.276), 14% (2.17 μM, CI 2.03–2.30 vs. 1.91 μM, CI 1.81–2.01), and 10% (0.65, CI 0.60–0.70 vs. 0.59, CI 0.55–0.62), respectively, (p=0.050, 0.003, and 0.050, respectively, Welch's t test) in normotensive men under 50 years old, compared to normotensive women under 50 years old (Fig. 7B). These findings suggest that there is an increase in nSMase activity in hypertensive individuals; however, studies with inhibitors of other ceramide producers, such as ceramide synthases (Rodriguez-Cuenca *et al.*, 2015) and acid sphingomyelinase (Pavoine & Pecker, 2009), are needed to confirm this interpretation.

Acute Mechanically-Mediated Activation of nSMase

To provide further support for our ECT findings and demonstrate that nSMase is activated during stretch, we applied high-resolution fluorescent optical mapping of electrical activity during acute ventricular pressure loading on wildtype mice (Fig. 8). Using this model, Pfeiffer et al. previously demonstrated that acute myocardial stretch induces conduction velocity slowing (Pfeiffer *et al.*, 2014). We hypothesized that nSMase mediates this stretch-induced conduction slowing, which is supported by Shi et al.'s findings that nSMase inhibition prevents shear stress induced membrane depolarization in vascular tissue (Shi *et al.*, 2020) which could affect sodium channel activation and subsequent conduction velocity slowing. Acute stretch (10 min) via pressure loading of mouse left ventricle resulted in a 29% and 31% decrease in longitudinal (0.71, CI 0.67–0.76 vs. 1.00, CI 0.81–1.18) and transversal (0.69, CI 0.51–0.88 vs. 1.00, CI 0.63–1.38) conduction velocity, respectively (p<0.001, two-way ANOVA with *post-hoc* Bonferroni correction; Fig. 9A–B), normalized to baseline, with no change in conduction anisotropy in control (2.04, CI 0.91–3.17 at baseline vs. 2.1, CI 0.99–3.21 during loading, p=1.00, two-way ANOVA with *post-hoc* Bonferroni correction) and GW4869-treated ventricles (2.39, CI 1.92–2.86 at baseline vs. 2.39, CI 2.09–2.69 during loading, p=1.00, two-way ANOVA with *post-hoc* Bonferroni

correction). Upon unloading (20 min), both conduction velocities returned to baseline levels. More importantly, pre-treatment of mouse hearts with the nSMase inhibitor GW4869 (5 μM) completely prevented the effect of stretch-induced conduction velocity slowing ($p<0.001$, two-way ANOVA with *post-hoc* Bonferroni correction). Acute stretch also resulted in reversable decrease in maximum upstroke velocity ($(dV/dt)_{max}$; Fig. 9C) which was prevented by pre-treatment with GW4869 (9.63, CI 8.12–11.12 vs. 12.23, CI 10.90–13.55; $p=0.020$, two-way ANOVA with *post-hoc* Bonferroni correction). Furthermore, we observed a small but significant correlation between $(dV/dt)_{max}$ and conduction velocity ($r^2=0.38$, $p=0.033$, F test; Fig. 9D), which may suggest that the stretch-induced diminished activity of Na^+ channels is a contributor to the observed conduction slowing. These findings identify nSMase as a key mediator of stretch-induced cardiac conduction slowing that can be observed during acute cardiac pressure-overload.

Discussion

Although the cardioprotective effects of caveolae are well-documented (Patel *et al.*, 2007; Kozera *et al.*, 2009; Markandeya *et al.*, 2015; Turner *et al.*, 2022), it is unclear how caveolae loss occurs during cardiac pathologies accompanied by chronically elevated myocardial stretch. This gap in knowledge is exacerbated by a lack of cardiac models that can distinguish the mechanisms of mechanical stress over long periods of time from other factors that may also contribute to caveolae remodeling. Using hiPSC-based Engineered Cardiac Tissue (ECT) constructs, we developed an *in vitro* protocol for modeling stretch-induced changes in cardiac structure and function, including a reduction in caveolae-like structures. We showed that the effects of cyclic stretch on ECT plasma membrane organization recapitulates the effects observed in mice after transaortic constriction (Markandeya *et al.*, 2015; Wei *et al.*, 2017). Several important features support the validity of the human ECT model to advance our understanding of caveolae biology. First, absolute caveolae density is similar between mice and the human ECT model. Second, both TAC in mice and cyclic stretch of the ECT reduce the plasma membrane convolution index to a similar degree, with a comparable reduction in caveolae abundance. These data suggest that our ECT can model some of the effects of increased mechanical stress that may occur in an elevated mechanical loading context, while excluding the additive neurohormonal/inflammatory effects.

Leveraging this novel stretch protocol, we identified neutral sphingomyelinases (nSMase) as potent mechano-mediated regulators of cardiac caveolae, suggesting a possible pathological mediator of cardiac conditions when caveolae loss occurs and conversely, where caveolae overexpression would be therapeutic (Patel *et al.*, 2007; Markandeya *et al.*, 2015). Prior to this study, there has been limited research on nSMase in the heart (Hernandez *et al.*, 2000) with many studies utilizing non-cardiac cell types including but not limited to cultured skeletal myotubes (Moylan *et al.*, 2014), mesenchymal stem cells (Makdissy *et al.*, 2018), and various smooth muscle types (Czarny *et al.*, 2003). In the present study, we found that not only is nSMase expressed in engineered and adult human cardiac tissue (Fig. 2F), but it may also have an active role in mediating the long-term effects of stretch on cardiac function. We showed that nSMase inhibition via GW4869 prevents stretch-induced reduction of caveolae-like structures (Fig. 1F) and mitigates the associated functional

changes observed in stretched ECT (Fig. 3). As shown by Yu et al. in non-myocyte cells (Yu *et al.*, 2005), we suspect that nSMase mechano-activation converts caveolar sphingomyelin to ceramide which displaces cholesterol from caveolae, disrupting their formation. While the differences in efficacy of GW4869 between nSMase type is unknown, GW4869 likely has a stronger inhibitory effect on sarcolemmal nSMase2 and nSMase3 (Moylan *et al.*, 2014) than the intracellular nSMase1 since GW4869 localizes to plasma membranes (Vuckovic *et al.*, 2017). Furthermore, our RT-qPCR data demonstrate that nSMase3 (*SMPD4)* is the predominantly expressed caveolae-associated nSMase (Moylan *et al.*, 2014) in adult human and mouse ventricles and human ECT (Fig. 2F), suggesting that nSMase3 is likely the main contributor to the observed nSMase-mediated effects. Given the suggested cardioprotective role of caveolae in the context of various cardiac conditions, such as hypertrophy (Markandeya *et al.*, 2015), hypertension (Egorov *et al.*, 2019), and heart failure (Wright *et al.*, 2014), the identification of a mediator of caveolae loss provides an excellent drug target that could be utilized to mitigate the severity of these conditions. Previously, it has been postulated that caveolae abundance can only be modulated by altering availability of cholesterol via methyl-β-cyclodextrin (Kozera *et al.*, 2009), and caveolin (Galbiati *et al.*, 2001) and cavin (Hill *et al.*, 2008) scaffolding proteins using knockout or overexpression animal models. Our findings add a new dimension to caveolae regulation and highlight nSMase as an upstream, mechano-regulator of caveolar organization.

It is still unknown if nSMase is intrinsically mechanosensitive or mechano-activated since various mechano-associated chemicals such as angiotensin II (Bautista-Perez *et al.*, 2015), TNF-α (Moylan *et al.*, 2014), and ROS (Hernandez *et al.*, 2000) may increase nSMase activity. Given the undetectable levels of *TNF-α* mRNA, it is unlikely that ECT nSMase is being activated by TNF-α protein, suggesting that nSMase is only being activated by mechanical cues in our experimental conditions. However, it has been shown that stretch mechano-activates NOX2 to produce ROS (Prosser *et al.*, 2013), ROS can activate nSMase (Hernandez *et al.*, 2000), and that stretch increases ROS in our ECT media (Fig. 2C). Therefore, it is possible that mechanically mediated activation of nSMase is at least partially augmented via ROS.

We also found that cyclic stretch induces production of ROS and short-chain ceramides in ECT media and that GW4869 prevents the production of the latter (Fig. 2A and C). While data by others suggest that stretch is a key component in the generation of ROS and ceramide (Czarny *et al.*, 2003; Prosser *et al.*, 2013) our findings extend these observations to indicate that in the cardiac context, nSMase may be a key mediator of stretch-mediated short-chain ceramide production. These results were indirectly supported by the human lipidomic data available from the MIDUS) study that enabled us to show that middle-age and older adults with hypertension have significantly upregulated levels of specific ceramides in systemic circulation (Figs. 6–7).

Our contraction analyses strengthen the importance of caveolae in mediating β-adrenergic modulation of excitation-contraction coupling, implicating nSMase as a molecular mediator of stretch-induced blunting of β-adrenergic response. We found that our stretched ECT exhibit a blunted β-adrenergic contractile kinetic response which was prevented by nSMase inhibition (Fig. 3A–B). In addition, this blunted response is most pronounced between

25 to 100% contraction (Fig. 3F–G), which may indicate that the caveolae disruption is interfering with proteins involved in excitation-contraction coupling rather than Ca^{2+} reuptake during relaxation phase. Given the limited increase in fibrosis (Fig. 5B) and no changes in sarcomere length in our stretched ECT (Fig. 1H), we conclude that the effect is likely due to loss of caveolar structures via elevated nSMase activity, but do not discount the possible additive role of fibrosis. However, our ECT stretch platform may not fully recapitulate animal models since our ECT lack neurohormonal factors such as angiotensin II, TNF-α, and catecholamines, which may potentiate stretch-induced fibrosis.

The effect of mechanical stress on cardiomyocytes is well-documented, with various groups demonstrating that increased mechanical stress, either by increased pressure (Pfeiffer *et al.*, 2014), swelling (Kozera *et al.*, 2009; Turner *et al.*, 2022), or physical stretch (Egorov *et al.*, 2019; MacDonald *et al.*, 2020; Khokhlova *et al.*, 2022; Peyronnet *et al.*, 2022) can disrupt cardiac conduction, induce apoptosis and arrhythmia, and alter cardiomyocyte tension and contraction. Supporting the relevance of nSMase in native tissue, our optical mapping experiments revealed that stretch-induced conduction velocity slowing is mediated by nSMase activation (Figs. 8 and 9). However, the underlying molecular mechanisms of stretch-induced conduction slowing remains unknown. Pfeiffer et al. found in neonatal murine cardiomyocytes that intact caveolae are required for stretch-induced conduction slowing (Pfeiffer *et al.*, 2014). Stretch also increases in intracellular ceramides (Shi *et al.*, 2020; Huang *et al.*, 2022), as well as caveolae disruption (Markandeya *et al.*, 2023) and altered membrane lipid composition (Boland & Drzewiecki, 2008), which could directly affect various ion channels involved in action potential propagation. For example, we found in rat pulmonary vein myocardium that stretch results in activation of volume-sensitive, inward chloride current $I_{Cl,swell}$, leading to membrane resting potential depolarization and intra-vein conduction slowing (Egorov *et al.*, 2019), likely via depolarization-mediated decrease in availability of Na^+ channels. Furthermore, exogenous and endogenous ceramides elicit $I_{Cl,swell}$ in rabbit ventricular myocytes (Raucci *et al.*, 2010) suggesting an nSMase-related mechanism. However, it is unknown whether stretch-induced activation of $I_{Cl,swell}$ leads to resting membrane depolarization and conduction slowing in ventricular myocardium. Indeed, it has been shown that isolated ventricular myocytes have limited swelling-induced resting potential depolarization (by ~3–5 mV) and only a negligible contribution of $I_{Cl,swell}$ to these changes (Ren *et al.*, 2008). Importantly, ceramide can also reduce I_{Na} (Huang *et al.*, 2022) and is involved in the activation of mechanosensitive cation (predominantly, Ca^{2+}) PIEZO1 channels (Shi *et al.*, 2020), although stretch-induced ventricular conduction slowing has been found to be insensitive to PIEZO1 inhibitor GsMTx-4 (Pfeiffer *et al.*, 2014). In addition, Pfeiffer et al. showed a significant increase in sarcolemmal lipid density during stretch (Pfeiffer *et al.*, 2014), suggesting the addition of material from sub-sarcolemmal caveolar stores to the sarcolemma, which could subsequently decrease the activity of Na^+ channels (Boland & Drzewiecki, 2008) and lead to conduction velocity slowing. Indeed, our analysis demonstrates reduced $(dV/dt)_{max}$ in stretched hearts that is prevented by nSMase inhibition (Fig. 9C). Furthermore, we show that this decrease in $(dV/dt)_{max}$ is significantly correlated to decreases in conduction velocity during loading (Fig. 9D). These data suggest that mechanically mediated activation of nSMase in loaded mouse hearts may involve reduced I_{Na}, either by caveolae loss or direct

action of ceramide on sodium channels. However, we also acknowledge the possible effect of stretch-induced nSMase activation on gap junctions and subsequent effects on conduction velocity. Upham et al. found in non-cardiac cells that membrane-permeable ceramides reduce gap junctional intercellular communication as measured by cell-to-cell dye transfer (Upham *et al.*, 2003).

Overall, we have developed a novel stretch protocol for inducing loss of caveolae-like structures in a human-based *in vitro* model that recapitulates the membrane morphology observed in spontaneously hypertensive rats and TAC mice. This model induces a loss in β-adrenergic contractile kinetic response that is similarly observed during heart failure and hypertrophy induced by hypertension. We leveraged this ECT model and an acute volume overload mouse model to identify nSMase as a potent mediator in stretch-induced caveolae loss and reduced cardiac function due to mechanical stress.

Study Limitations

Notwithstanding the importance and novelty of our findings, we acknowledge the limitations of the ECT stretch model due to several factors, including the relative maturity of our differentiated iPSC-myocytes, a relatively high baseline fibrosis compared to healthy human ventricular myocardium (Unverferth *et al.*, 1986), the absence of resident immune cells, circulating inflammatory and neurohormonal factors, and the duration of the stretch protocol used. These factors may have contributed to the limited changes in both percent area fibrosis and fibrotic mRNA and the inability to detect mRNA for inflammatory cytokines (Fig. 5). For these reasons, our ECT stretch model may not fully recapitulate native cardiac hypertension or hypertrophy but can be used to test hypotheses regarding molecular mediators and processes related to chronically elevated stretch. Using this model, we were able to dissect specific mechanisms of nSMase mechanically-mediated activation and factors that react to cardiac mechanical stress but recognize that due to the presence of other inflammatory factors including TNF-α (Moylan *et al.*, 2014), we may expect that nSMase activation is further elevated in native hypertensive myocardium. Lastly, given that GW4869 is also a blocker of exosome generation, we acknowledge the possibility that prevention of paracrine signaling could play a role in the effects that we observed or other nonspecific effects.

Acknowledgements

The author(s) thank the UW-Madison Translational Research Initiatives in Pathology laboratory (TRIP), supported by the UW Department of Pathology and Laboratory Medicine, UWCCC (P30 CA014520) and the Office of The Director-NIH (S10 OD023526) for use of its facilities and services. Finally, we thank Randall J. Massey and the SMPH Electron Microscopy Facility (UW-Madison) for critical assistance in preparing and imaging ECTs, and Janay Walters for manuscript editing and suggestions.

Funding

This work was supported by grants from National Institutes of Health R01HL141214, R01HL139738, R01HL146652, American Heart Association Career Development Award 16SDG29120011, and the Wisconsin Partnership Program 4140 to A.V.G. D.G.P.T. would like to acknowledge the NIH Predoctoral Training grant T32GM008688, support provided by the University of Wisconsin-Madison Office of the Vice Chancellor for Research and Graduate Education with funding from the Wisconsin Alumni Research Foundation, and an American Heart Association Predoctoral Fellowship (903203). Y.G. would like to acknowledge National Institutes of Health

R01 GM125085, R01 HL096971, GM117058 and S10 OD018475. The MIDUS project was supported by awards from the National Institute on Aging (P01 AG030166, U19AG051426).

Biography

Daniel G.P Turner is a 5th-year graduate student studying molecular and cellular pharmacology in Dr. Alexey Glukhov's lab at University of Wisconsin-Madison. He is anticipating his thesis defense in early 2024 focused on regulation of cardiac caveolae. A participant in Wisconsin's prominent dairy science and industry, he previously gained experience at The Center for Dairy Research in Madison, WI. He looks forward to utilizing his experience in disease modeling via engineered cardiac tissue to better identify factors involved in various cardiac pathologies.

Data availability

The datasets generated during and/or analyzed during the current study are available from the corresponding author on reasonable request, with exception to human ceramide data where permission must be obtained through MIDUS.

References

Atkins FL, Bing OH, DiMauro PG, Conrad CH, Robinson KG & Brooks WW. (1995). Modulation of left and right ventricular beta-adrenergic receptors from spontaneously hypertensive rats with left ventricular hypertrophy and failure. Hypertension 26, 78–82. [PubMed: 7607736]

Bautista-Perez R, del Valle-Mondragon L, Cano-Martinez A, Perez-Mendez O, Escalante B & Franco M. (2015). Involvement of neutral sphingomyelinase in the angiotensin II signaling pathway. Am J Physiol Renal Physiol 308, F1178–1187. [PubMed: 25354938]

Berkowitz L, Salazar C, Ryff CD, Coe CL & Rigotti A. (2022). Serum sphingolipid profiling as a novel biomarker for metabolic syndrome characterization. Front Cardiovasc Med 9, 1092331. [PubMed: 36578837]

Boland LM & Drzewiecki MM. (2008). Polyunsaturated fatty acid modulation of voltage-gated ion channels. Cell Biochem Biophys 52, 59–84. [PubMed: 18830821]

Böhm M, Diet F, Feiler G, Kemkes B, Kreuzer E, Weinhold C & Erdmann E. (1988). Subsensitivity of the failing human heart to isoprenaline and milrinone is related to beta-adrenoceptor downregulation. J Cardiovasc Pharmacol 12, 726–732. [PubMed: 2467092]

Calaghan S & White E. (2006). Caveolae modulate excitation-contraction coupling and beta2-adrenergic signalling in adult rat ventricular myocytes. Cardiovasc Res 69, 816–824. [PubMed: 16318846]

Chen Y, Pat B, Zheng J, Cain L, Powell P, Shi K, Sabri A, Husain A & Dell'italia LJ. (2010). Tumor necrosis factor-alpha produced in cardiomyocytes mediates a predominant myocardial inflammatory response to stretch in early volume overload. J Mol Cell Cardiol 49, 70–78. [PubMed: 20045005]

Colligan PB, Relling DP & Ren J. (2002). Ceramide attenuates high glucose-induced cardiac contractile abnormalities in cultured adult rat ventricular myocytes. Cell Mol Biol (Noisy-le-grand) 48 Online Pub, OL251–257. [PubMed: 12643441]

Czarny M, Liu J, Oh P & Schnitzer JE. (2003). Transient mechanoactivation of neutral sphingomyelinase in caveolae to generate ceramide. J Biol Chem 278, 4424–4430. [PubMed: 12473648]

De Lange WJ, Farrell ET, Hernandez JJ, Stempien A, Kreitzer CR, Jacobs DR, Petty DL, Moss RL, Crone WC & Ralphe JC. (2023). cMyBP-C ablation in human engineered cardiac tissue causes progressive Ca2+-handling abnormalities. J Gen Physiol 155.

de Lange WJ, Farrell ET, Kreitzer CR, Jacobs DR, Lang D, Glukhov AV & Ralphe JC. (2021). Human iPSC-engineered cardiac tissue platform faithfully models important cardiac physiology. Am J Physiol Heart Circ Physiol 320, H1670–H1686. [PubMed: 33606581]

Díez J (2007). Mechanisms of cardiac fibrosis in hypertension. J Clin Hypertens (Greenwich) 9, 546–550. [PubMed: 17617765]

Egorov YV, Lang D, Tyan L, Turner D, Lim E, Piro ZD, Hernandez JJ, Lodin R, Wang R, Schmuck EG, Raval AN, Ralphe CJ, Kamp TJ, Rosenshtraukh LV & Glukhov AV. (2019). Caveolae-Mediated Activation of Mechanosensitive Chloride Channels in Pulmonary Veins Triggers Atrial Arrhythmogenesis. J Am Heart Assoc 8, e012748. [PubMed: 31597508]

Galbiati F, Engelman JA, Volonte D, Zhang XL, Minetti C, Li M, Hou H Jr., Kneitz B, Edelmann W & Lisanti MP. (2001). Caveolin-3 null mice show a loss of caveolae, changes in the microdomain distribution of the dystrophin-glycoprotein complex, and t-tubule abnormalities. J Biol Chem 276, 21425–21433. [PubMed: 11259414]

Gao HL, Yu XJ, Hu HB, Yang QW, Liu KL, Chen YM, Zhang Y, Zhang DD, Tian H, Zhu GQ, Qi J & Kang YM. (2021). Apigenin Improves Hypertension and Cardiac Hypertrophy Through Modulating NADPH Oxidase-Dependent ROS Generation and Cytokines in Hypothalamic Paraventricular Nucleus. Cardiovasc Toxicol 21, 721–736. [PubMed: 34076830]

Glukhov AV, Fedorov VV, Kalish PW, Ravikumar VK, Lou Q, Janks D, Schuessler RB, Moazami N & Efimov IR. (2012). Conduction remodeling in human end-stage nonischemic left ventricular cardiomyopathy. Circulation 125, 1835–1847. [PubMed: 22412072]

Glukhov AV, Flagg TP, Fedorov VV, Efimov IR & Nichols CG. (2010). Differential K(ATP) channel pharmacology in intact mouse heart. J Mol Cell Cardiol 48, 152–160. [PubMed: 19744493]

He L, Kim T, Long Q, Liu J, Wang P, Zhou Y, Ding Y, Prasain J, Wood PA & Yang Q. (2012). Carnitine palmitoyltransferase-1b deficiency aggravates pressure overload-induced cardiac hypertrophy caused by lipotoxicity. Circulation 126, 1705–1716. [PubMed: 22932257]

Hernandez OM, Discher DJ, Bishopric NH & Webster KA. (2000). Rapid activation of neutral sphingomyelinase by hypoxia-reoxygenation of cardiac myocytes. Circ Res 86, 198–204. [PubMed: 10666416]

Hill MM, Bastiani M, Luetterforst R, Kirkham M, Kirkham A, Nixon SJ, Walser P, Abankwa D, Oorschot VM, Martin S, Hancock JF & Parton RG. (2008). PTRF-Cavin, a conserved cytoplasmic protein required for caveola formation and function. Cell 132, 113–124. [PubMed: 18191225]

Huang SY, Lu YY, Lin YK, Chen YC, Chen YA, Chung CC, Lin WS, Chen SA & Chen YJ. (2022). Ceramide modulates electrophysiological characteristics and oxidative stress of pulmonary vein cardiomyocytes. Eur J Clin Invest 52, e13690. [PubMed: 34662431]

Jensen PN, Fretts AM, Hoofnagle AN, Sitlani CM, McKnight B, King IB, Siscovick DS, Psaty BM, Heckbert SR, Mozaffarian D, Sotoodehnia N & Lemaitre RN. (2020). Plasma Ceramides and Sphingomyelins in Relation to Atrial Fibrillation Risk: The Cardiovascular Health Study. J Am Heart Assoc 9, e012853. [PubMed: 32019406]

Ji R, Akashi H, Drosatos K, Liao X, Jiang H, Kennel PJ, Brunjes DL, Castillero E, Zhang X, Deng LY, Homma S, George IJ, Takayama H, Naka Y, Goldberg IJ & Schulze PC. (2017). Increased de novo ceramide synthesis and accumulation in failing myocardium. JCI Insight 2.

Jiang G, Gong H, Niu Y, Yang C, Wang S, Chen Z, Ye Y, Zhou N, Zhang G, Ge J & Zou Y. (2015). Identification of Amino Acid Residues in Angiotensin II Type 1 Receptor Sensing Mechanical Stretch and Function in Cardiomyocyte Hypertrophy. Cell Physiol Biochem 37, 105–116. [PubMed: 26303226]

Kauhanen D, Sysi-Aho M, Koistinen KM, Laaksonen R, Sinisalo J & Ekroos K. (2016). Development and validation of a high-throughput LC-MS/MS assay for routine measurement of molecular ceramides. Anal Bioanal Chem 408, 3475–3483. [PubMed: 26922344]

Khokhlova A, Solovyova O, Kohl P & Peyronnet R. (2022). Single cardiomyocytes from papillary muscles show lower preload-dependent activation of force compared to cardiomyocytes from the left ventricular free wall. J Mol Cell Cardiol 166, 127–136. [PubMed: 35248551]

Kozera L, White E & Calaghan S. (2009). Caveolae act as membrane reserves which limit mechanosensitive I(Cl,swell) channel activation during swelling in the rat ventricular myocyte. PLoS One 4, e8312. [PubMed: 20011535]

Lian X, Zhang J, Azarin SM, Zhu K, Hazeltine LB, Bao X, Hsiao C, Kamp TJ & Palecek SP. (2013). Directed cardiomyocyte differentiation from human pluripotent stem cells by modulating Wnt/β-catenin signaling under fully defined conditions. Nat Protoc 8, 162–175. [PubMed: 23257984]

Lu K, Seidel T, Cao-Ehlker X, Dorn T, Batcha AMN, Schneider CM, Semmler M, Volk T, Moretti A, Dendorfer A & Tomasi R. (2021). Progressive stretch enhances growth and maturation of 3D stem-cell-derived myocardium. Theranostics 11, 6138–6153. [PubMed: 33995650]

MacDonald EA, Madl J, Greiner J, Ramadan AF, Wells SM, Torrente AG, Kohl P, Rog-Zielinska EA & Quinn TA. (2020). Sinoatrial Node Structure, Mechanics, Electrophysiology and the Chronotropic Response to Stretch in Rabbit and Mouse. Front Physiol 11, 809. [PubMed: 32774307]

Makdissy N, Haddad K, AlBacha JD, Chaker D, Ismail B, Azar A, Oreibi G, Ayoub D, Achkar I, Quilliot D & Fajloun Z. (2018). Essential role of ATP6AP2 enrichment in caveolae/lipid raft microdomains for the induction of neuronal differentiation of stem cells. Stem Cell Res Ther 9, 132. [PubMed: 29751779]

Markandeya YS, Gregorich ZR, Feng L, Ramchandran V, O' Hara T, Vaidyanathan R, Mansfield C, Keefe AM, Beglinger CJ, Best JM, Kalscheur MM, Lea MR, Hacker TA, Gorelik J, Trayanova NA, Eckhardt LL, Makielski JC, Balijepalli RC & Kamp TJ. (2023). Caveolin-3 and Caveolae regulate ventricular repolarization. J Mol Cell Cardiol 177, 38–49. [PubMed: 36842733]

Markandeya YS, Phelan LJ, Woon MT, Keefe AM, Reynolds CR, August BK, Hacker TA, Roth DM, Patel HH & Balijepalli RC. (2015). Caveolin-3 Overexpression Attenuates Cardiac Hypertrophy via Inhibition of T-type Ca2+ Current Modulated by Protein Kinase Calpha in Cardiomyocytes. J Biol Chem 290, 22085–22100. [PubMed: 26170457]

Moylan JS, Smith JD, Wolf Horrell EM, McLean JB, Deevska GM, Bonnell MR, Nikolova-Karakashian MN & Reid MB. (2014). Neutral sphingomyelinase-3 mediates TNF-stimulated oxidant activity in skeletal muscle. Redox Biol 2, 910–920. [PubMed: 25180167]

Parton RG & del Pozo MA. (2013). Caveolae as plasma membrane sensors, protectors and organizers. Nat Rev Mol Cell Biol 14, 98–112. [PubMed: 23340574]

Parton RG & Simons K. (2007). The multiple faces of caveolae. Nat Rev Mol Cell Biol 8, 185–194. [PubMed: 17318224]

Parton RG, Tillu VA & Collins BM. (2018). Caveolae. Curr Biol 28, R402–R405. [PubMed: 29689223]

Patel HH, Tsutsumi YM, Head BP, Niesman IR, Jennings M, Horikawa Y, Huang D, Moreno AL, Patel PM, Insel PA & Roth DM. (2007). Mechanisms of cardiac protection from ischemia/reperfusion injury: a role for caveolae and caveolin-1. FASEB J 21, 1565–1574. [PubMed: 17272740]

Pavoine C & Pecker F. (2009). Sphingomyelinases: their regulation and roles in cardiovascular pathophysiology. Cardiovasc Res 82, 175–183. [PubMed: 19176603]

Peyronnet R, Desai A, Edelmann JC, Cameron BA, Emig R, Kohl P & Dean D. (2022). Simultaneous assessment of radial and axial myocyte mechanics by combining atomic force microscopy and carbon fibre techniques. Philos Trans R Soc Lond B Biol Sci 377, 20210326. [PubMed: 36189808]

Pfeiffer ER, Wright AT, Edwards AG, Stowe JC, McNall K, Tan J, Niesman I, Patel HH, Roth DM, Omens JH & McCulloch AD. (2014). Caveolae in ventricular myocytes are required for stretch-dependent conduction slowing. J Mol Cell Cardiol 76, 265–274. [PubMed: 25257915]

Prosser BL, Ward CW & Lederer WJ. (2013). X-ROS signalling is enhanced and graded by cyclic cardiomyocyte stretch. Cardiovasc Res 98, 307–314. [PubMed: 23524301]

Raucci FJ Jr., Wijesinghe DS, Chalfant CE & Baumgarten CM. (2010). Exogenous and endogenous ceramides elicit volume-sensitive chloride current in ventricular myocytes. Cardiovasc Res 86, 55–62. [PubMed: 20008476]

Ren Z, Raucci FJ, Browe DM & Baumgarten CM. (2008). Regulation of swelling-activated Cl(−) current by angiotensin II signalling and NADPH oxidase in rabbit ventricle. Cardiovasc Res 77, 73–80. [PubMed: 18006461]

Rodriguez-Cuenca S, Barbarroja N & Vidal-Puig A. (2015). Dihydroceramide desaturase 1, the gatekeeper of ceramide induced lipotoxicity. Biochim Biophys Acta 1851, 40–50. [PubMed: 25283058]

Roth GA, Mensah GA, Johnson CO, Addolorato G, Ammirati E, Baddour LM, Barengo NC, Beaton AZ, Benjamin EJ, Benziger CP, Bonny A, Brauer M, Brodmann M, Cahill TJ, Carapetis J, Catapano AL, Chugh SS, Cooper LT, Coresh J, Criqui M, DeCleene N, Eagle KA, Emmons-Bell S, Feigin VL, Fernández-Solà J, Fowkes G, Gakidou E, Grundy SM, He FJ, Howard G, Hu F, Inker L, Karthikeyan G, Kassebaum N, Koroshetz W, Lavie C, Lloyd-Jones D, Lu HS, Mirijello A, Temesgen AM, Mokdad A, Moran AE, Muntner P, Narula J, Neal B, Ntsekhe M, Moraes de Oliveira G, Otto C, Owolabi M, Pratt M, Rajagopalan S, Reitsma M, Ribeiro ALP, Rigotti N, Rodgers A, Sable C, Shakil S, Sliwa-Hahnle K, Stark B, Sundström J, Timpel P, Tleyjeh IM, Valgimigli M, Vos T, Whelton PK, Yacoub M, Zuhlke L, Murray C, Fuster V & Group G-N-JGBoCDW. (2020). Global Burden of Cardiovascular Diseases and Risk Factors, 1990–2019: Update From the GBD 2019 Study. J Am Coll Cardiol 76, 2982–3021. [PubMed: 33309175]

Rybin VO, Pak E, Alcott S & Steinberg SF. (2003). Developmental changes in beta2-adrenergic receptor signaling in ventricular myocytes: the role of Gi proteins and caveolae microdomains. Mol Pharmacol 63, 1338–1348. [PubMed: 12761344]

Shi J, Hyman AJ, De Vecchis D, Chong J, Lichtenstein L, Futers TS, Rouahi M, Salvayre AN, Auge N, Kalli AC & Beech DJ. (2020). Sphingomyelinase Disables Inactivation in Endogenous PIEZO1 Channels. Cell Rep 33, 108225. [PubMed: 33027663]

Turner DGP, Tyan L, DeGuire FC, Medvedev RY, Stroebel SJ, Lang D & Glukhov AV. (2022). Caveolin-3 prevents swelling-induced membrane damage via regulation of ICl,swell activity. Biophys J 121, 1643–1659. [PubMed: 35378081]

Ulmer CZ, Jones CM, Yost RA, Garrett TJ & Bowden JA. (2018). Optimization of Folch, Bligh-Dyer, and Matyash sample-to-extraction solvent ratios for human plasma-based lipidomics studies. Anal Chim Acta 1037, 351–357. [PubMed: 30292311]

Unverferth DV, Baker PB, Swift SE, Chaffee R, Fetters JK, Uretsky BF, Thompson ME & Leier CV. (1986). Extent of myocardial fibrosis and cellular hypertrophy in dilated cardiomyopathy. Am J Cardiol 57, 816–820. [PubMed: 2938462]

Upham BL, Koski TR, Rummel AM, Wilson MR, Horvath A & Trosko JE. (2003). Differential roles of 2, 6, and 8 carbon ceramides on the modulation of gap junctional communication and apoptosis during carcinogenesis. Cancer Lett 191, 27–34. [PubMed: 12609706]

Vuckovic S, Vandyke K, Rickards DA, McCauley Winter P, Brown SHJ, Mitchell TW, Liu J, Lu J, Askenase PW, Yuriev E, Capuano B, Ramsland PA, Hill GR, Zannettino ACW & Hutchinson AT. (2017). The cationic small molecule GW4869 is cytotoxic to high phosphatidylserine-expressing myeloma cells. Br J Haematol 177, 423–440. [PubMed: 28211573]

Wei EQ, Sinden DS, Mao L, Zhang H, Wang C & Pitt GS. (2017). Inducible Fgf13 ablation enhances caveolae-mediated cardioprotection during cardiac pressure overload. Proc Natl Acad Sci U S A 114, E4010–E4019. [PubMed: 28461495]

Wright PT, Nikolaev VO, O'Hara T, Diakonov I, Bhargava A, Tokar S, Schobesberger S, Shevchuk AI, Sikkel MB, Wilkinson R, Trayanova NA, Lyon AR, Harding SE & Gorelik J. (2014). Caveolin-3 regulates compartmentation of cardiomyocyte beta2-adrenergic receptor-mediated cAMP signaling. J Mol Cell Cardiol 67, 38–48. [PubMed: 24345421]

Wu BX, Clarke CJ & Hannun YA. (2010). Mammalian neutral sphingomyelinases: regulation and roles in cell signaling responses. Neuromolecular Med 12, 320–330. [PubMed: 20552297]

Wu Q, Sun L, Hu X, Wang X, Xu F, Chen B, Liang X, Xia J, Wang P, Aibara D, Zhang S, Zeng G, Yun C, Yan Y, Zhu Y, Bustin M, Gonzalez FJ & Jiang C. (2021). Suppressing the intestinal farnesoid X receptor/sphingomyelin phosphodiesterase 3 axis decreases atherosclerosis. J Clin Invest 131.

Yu C, Alterman M & Dobrowsky RT. (2005). Ceramide displaces cholesterol from lipid rafts and decreases the association of the cholesterol binding protein caveolin-1. J Lipid Res 46, 1678–1691. [PubMed: 15863835]

Zhang H, Huang W, Liu H, Zheng Y & Liao L. (2020). Mechanical stretching of pulmonary vein stimulates matrix metalloproteinase-9 and transforming growth factor-β1 through stretch-activated channel/MAPK pathways in pulmonary hypertension due to left heart disease model rats. PLoS One 15, e0235824. [PubMed: 32881898]

Zhang J, Klos M, Wilson GF, Herman AM, Lian X, Raval KK, Barron MR, Hou L, Soerens AG, Yu J, Palecek SP, Lyons GE, Thomson JA, Herron TJ, Jalife J & Kamp TJ. (2012). Extracellular matrix promotes highly efficient cardiac differentiation of human pluripotent stem cells: the matrix sandwich method. Circ Res 111, 1125–1136. [PubMed: 22912385]

Zhang J, Tao R, Campbell KF, Carvalho JL, Ruiz EC, Kim GC, Schmuck EG, Raval AN, da Rocha AM, Herron TJ, Jalife J, Thomson JA & Kamp TJ. (2019). Functional cardiac fibroblasts derived from human pluripotent stem cells via second heart field progenitors. Nat Commun 10, 2238. [PubMed: 31110246]

Key Points

- We have developed a novel stretch protocol for human engineered cardiac tissue that recapitulates changes in plasma membrane morphology observed in animal models of pressure/volume overload.
- ECT stretch induces nSMase activation, ceramide generation, and caveolae disassembly.
- nSMase activation blunts cardiac β-adrenergic contractile kinetics and mediates stretch-induced slowing of conduction and upstroke velocity.
- Circulating ceramides are increased in adults with hypertension, highlighting the clinical relevance of stretch-induced nSMase activity.

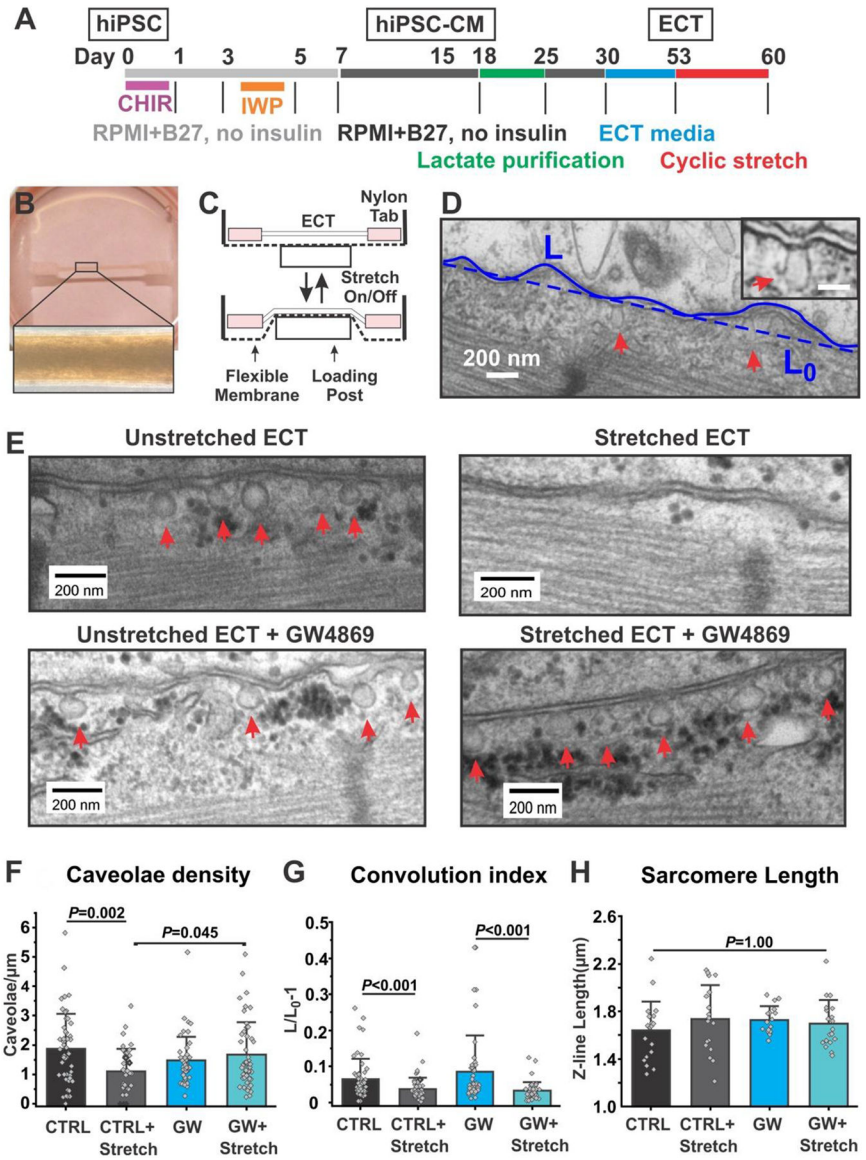

Fig. 1: Cyclic stretch reduces the density of caveolae-like structures via nSMase.

A – Timeline for hiPSC-CM differentiation via GiWi protocol, hiPSC-CM purification, ECT generation, and ECT cyclic stretch. **B** – Representative ECT in Flexcell well and at 10x magnification. **C** – Mechanism of Flexcell stretch. **D** – Representative TEM image of ECT membrane at 40,000x. **E** – Representative TEM images of unstretched, stretched, and GW4869-treated ECTs, red arrows indicate caveolae-like structures at 40,000x. **F** – ECT caveolae-like structure density measurements. **G** – ECT convolution index measurements. **H** – ECT sarcomere length measurements. CTRL - unstretched with vehicle, CTRL+Stretch - stretched with vehicle, GW - unstretched with GW4869, GW+Stretch - stretched with GW4869. Significance determined by two-way ANOVA with *post-hoc* Bonferroni correction or Kruskal-Wallis tests. Mean (SD) are shown, n=4–5 ECT/group (8–10 unique cardiomyocyte membrane measurements per ECT from two different sections).

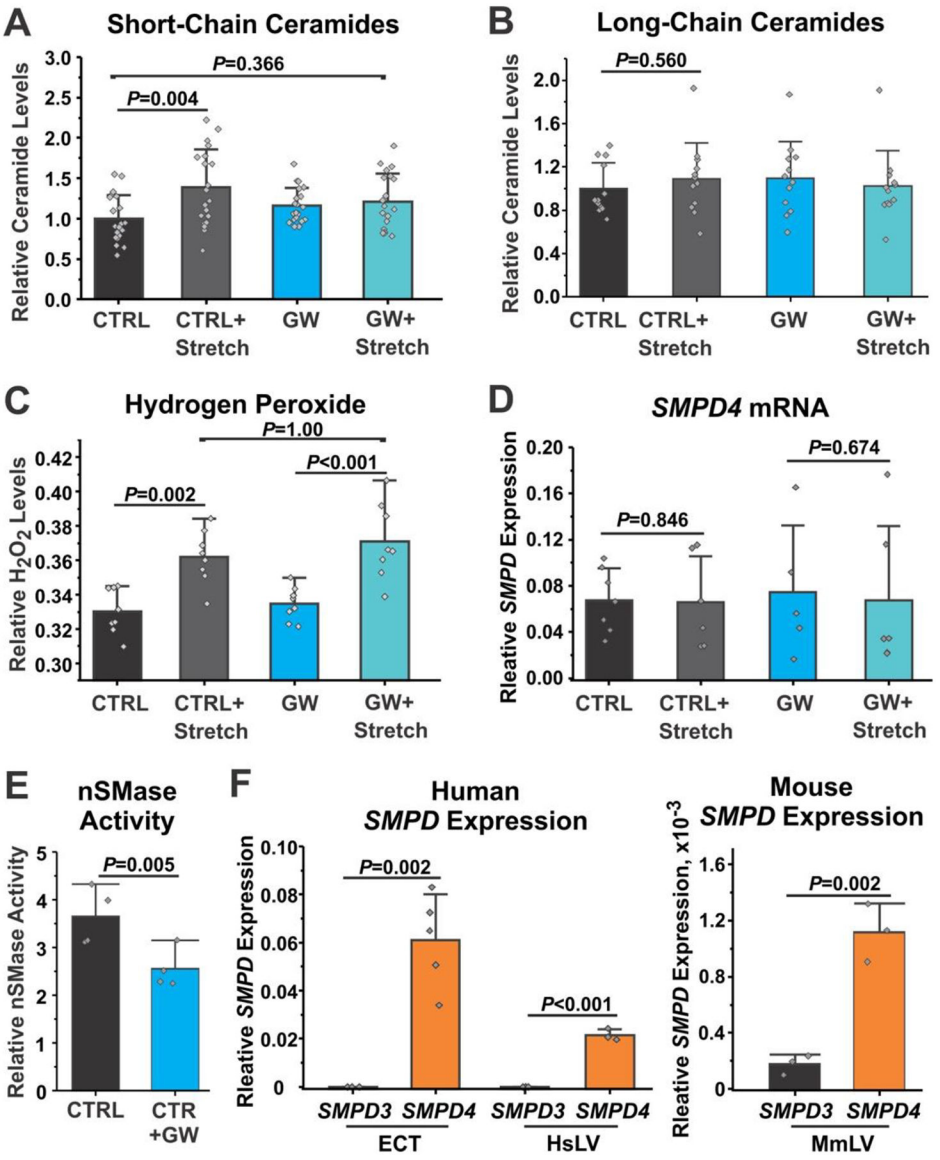

Fig. 2: Cyclic stretch induces production of ceramide via nSMase3 and ROS (nSMase-independent).

Relative levels of short-chain ceramides (**A**, acyl side chain <26) and long-chain ceramides (**B**, acyl side chain>26) from ECT cell culture media after 4 h of cyclic stretch. **C** – Relative H_2O_2 levels of ECT after 1 h of cyclic stretch. **D** – *SMPD4* mRNA expression relative to *GAPDH* in ECT. **E** – ECT nSMase activity with and without 20 μM GW4869. **F** – *SMPD* mRNA expression relative to *GAPDH* in ECT and human left ventricle (HsLV, *left*) and mouse left ventricle (MmLV, *right*). Significance determined via two-way ANOVA with *post-hoc* Bonferroni correction or Student's t test. Mean (SD) are shown. n=4 ECT media/group experiments, n=3–7 ECT/group for gene expression experiments, n=3 mice.

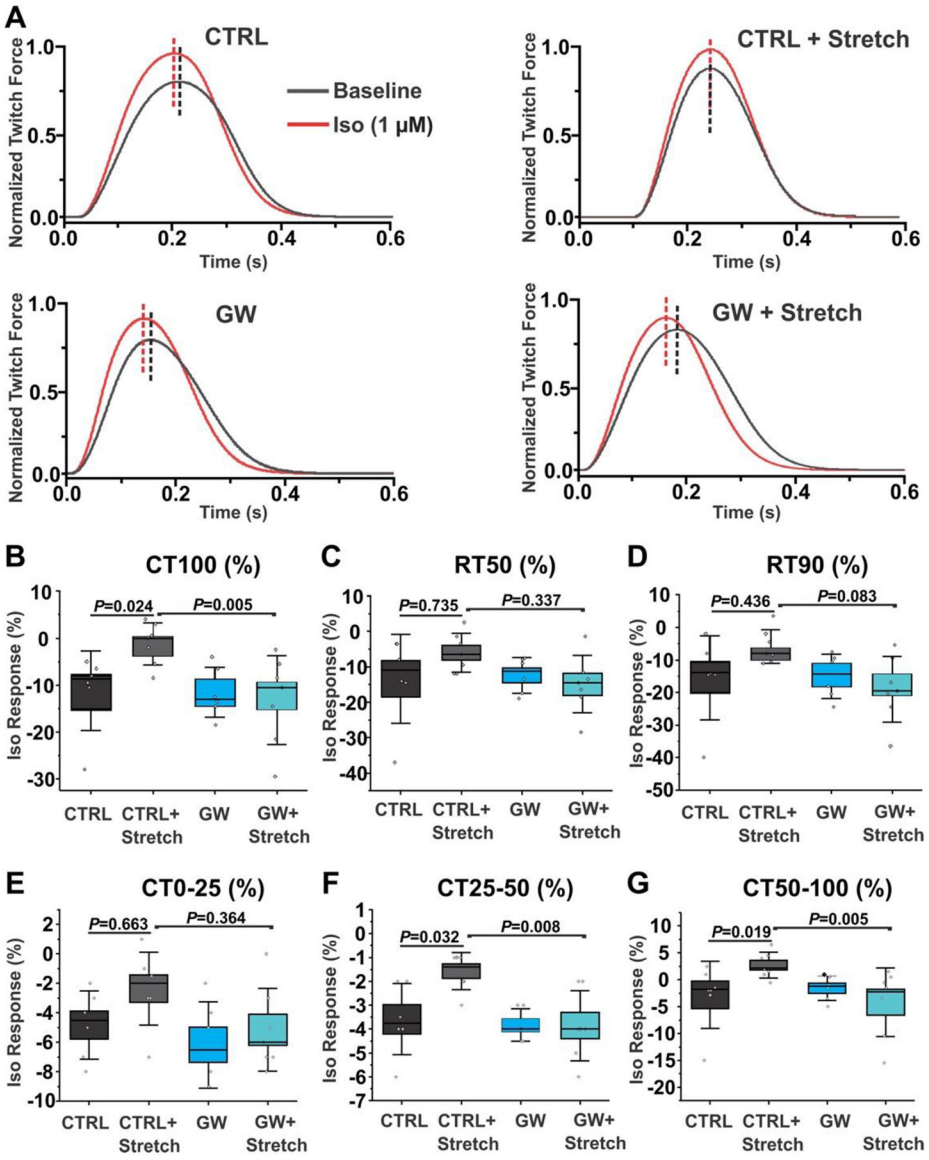

Fig. 3: Cyclic stretch blunts ECT β-adrenergic contractile kinetics in an nSMase-dependent manner.

A – Representative ECT contraction traces before and after 1 μM isoproterenol (Iso) paced at 1.5 Hz, vertical dotted lines indicate maximum contraction. Isoproterenol-induced change in ECT paced at 1.5 Hz in time to 100% contraction **(CT100, B)**, time to 50% relaxation **(RT50, C)**, time to 90% relaxation **(RT90, D)**, time for 0 to 25% contraction **(CT0–25, E)**, time for 25 to 50% contraction **(CT25–50, F)**, time for 50–100% contraction **(CT50–100, G)**. CTRL - unstretched with vehicle, CTRL+Stretch – stretched with vehicle, GW – unstretched with GW4869, GW+Stretch – stretched with GW4869. Significance was determined either with Kruskal-Wallis tests or two-way ANOVA with *post-hoc* Bonferroni correction. Mean (SD) are shown, n=6–7 ECT/group.

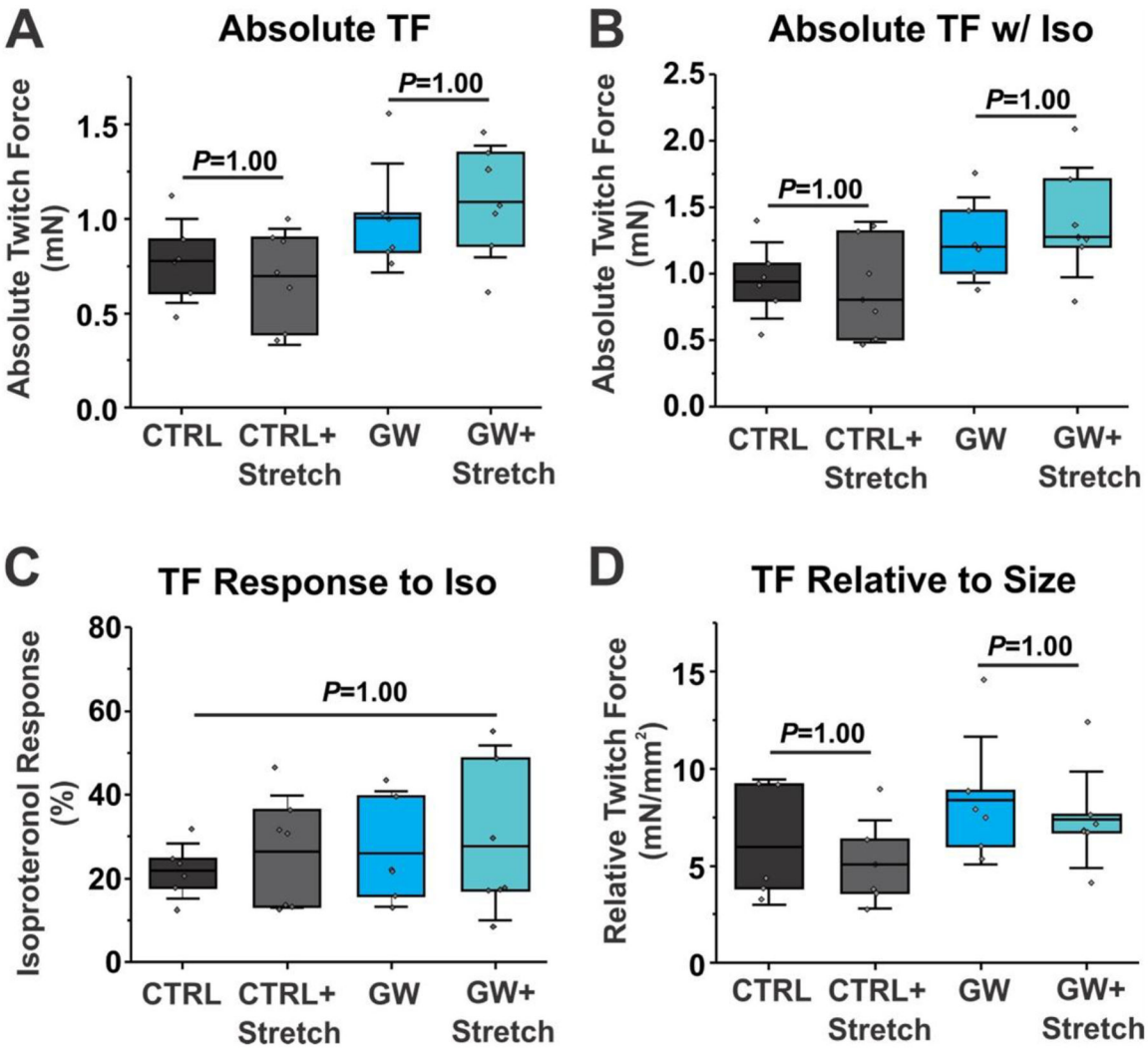

Fig. 4: Cyclic stretch and GW4869 have no effect on ECT twitch force.

Absolute ECT twitch force at baseline (**A**) and after 1 μM isoproterenol (**B**). ECT twitch force response to 1 μM isoproterenol (**C**) and relative to ECT size (**D**). CTRL – unstretched with vehicle, CTRL+Stretch – stretched with vehicle, GW – unstretched with GW4869, GW+Stretch – stretched with GW4869. Significance was determined via two-way ANOVA with *post-hoc* Bonferroni correction. Mean (SD) are shown, n=5–7 ECT/group.

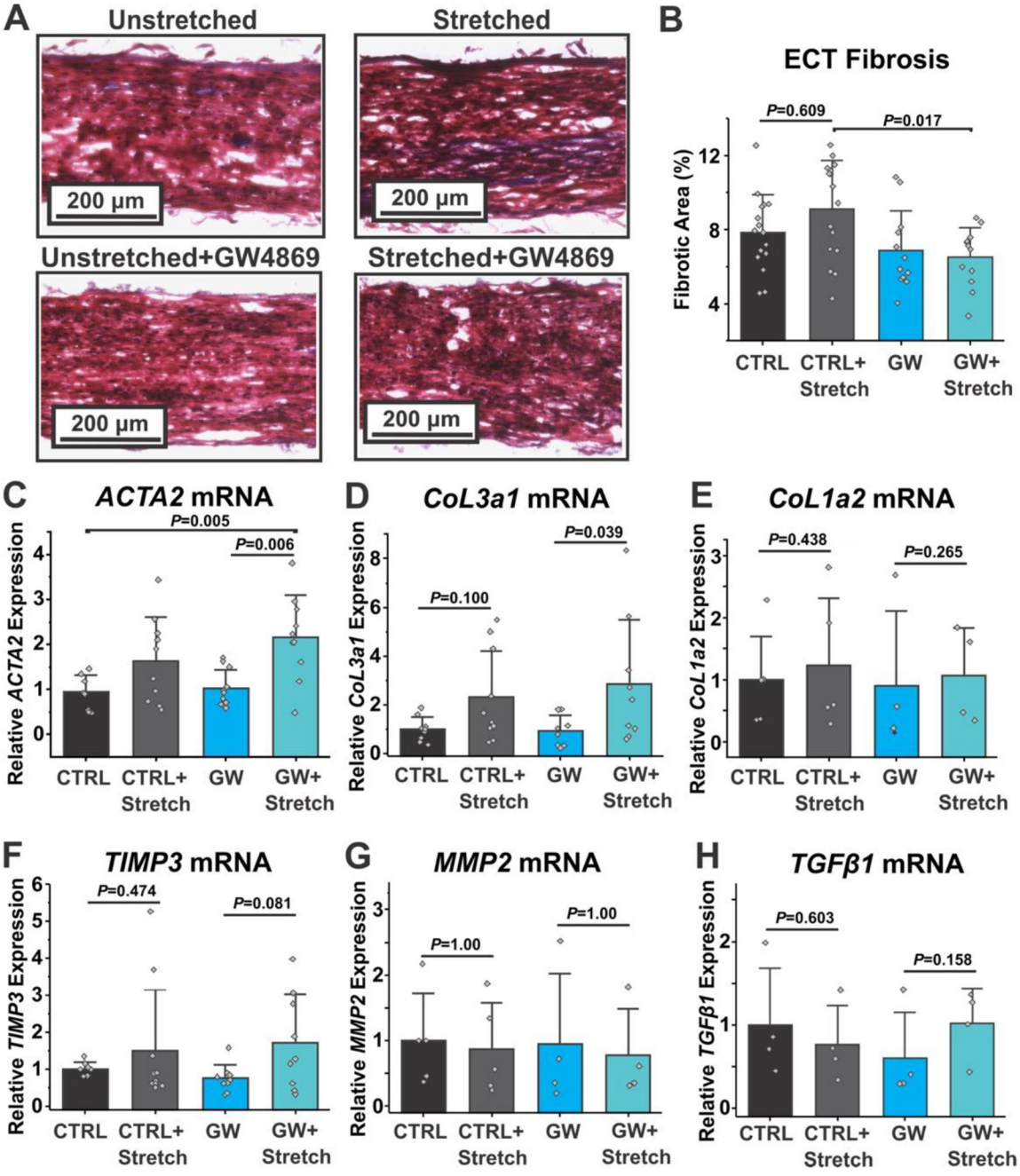

Fig. 5: Stretch has a limited effect on ECT fibrosis.

Representative Masson's trichrome staining ECT images (**A**) and quantification of fibrotic area percentage (**B**), n=3–4 ECT/group with four measurements from two sections per ECT. RT-qPCR analysis of *ACTA2* (**C**), *COL3A1* (**D**), *COL1A2* (**E**), *TIMP3* (**F**), *MMP2* (**G**), and *TGF-β1* (**H**), relative to *GAPDH*. N=4–10 ECT/group. CTRL – unstretched ECT with vehicle, GW – GW4869 treated ECT. Significance determined via two-way ANOVA with *post-hoc* Bonferroni or Kruskal-Wallis tests. Error bars are SD.

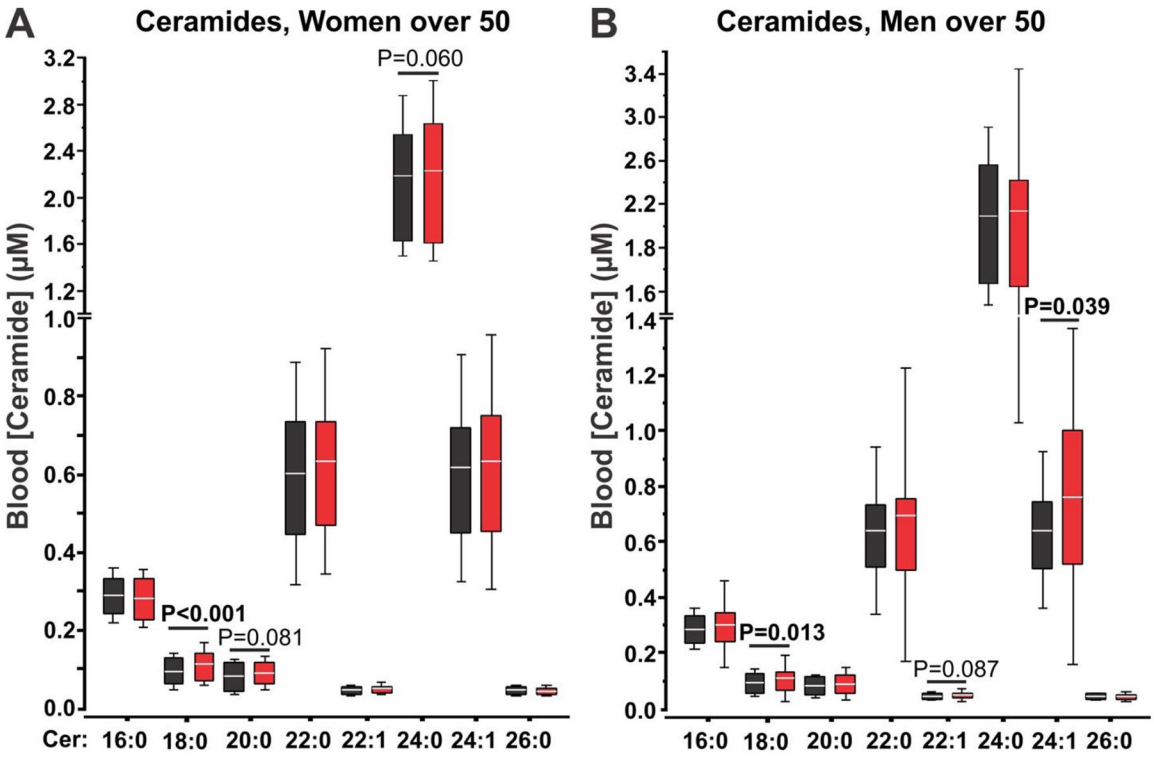

Fig. 6: Blood ceramide levels in American adults over 50 years old with and without hypertension.

Absolute ceramide concentrations (μM) of women and men over 50 years old (**A** and **B**, respectively). Significance determined via Welch's t test. Mean (SD) are shown. Black or red bars indicate normo- or hypertensive groups, respectively. n=60–200 human blood samples.

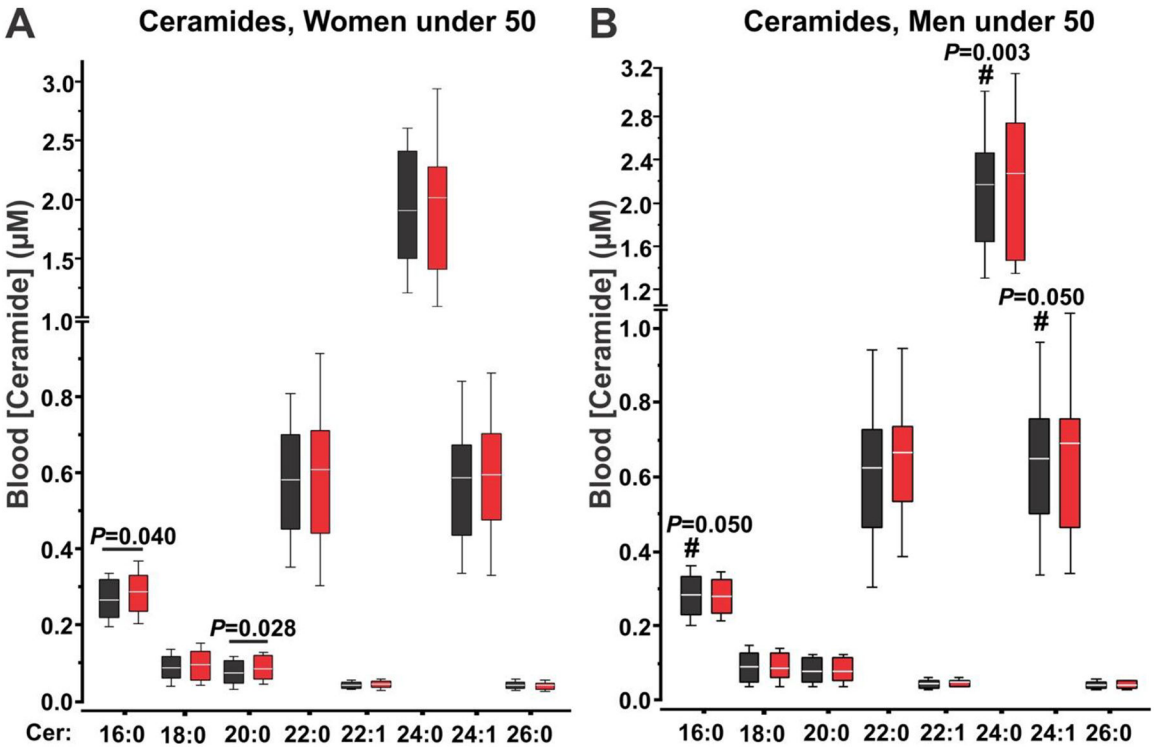

Fig. 7: Blood ceramide levels in American adults under 50 years old with and without hypertension.

Absolute ceramide concentrations (μM) of women and men under 50 years old (**A** and **B**, respectively). # indicates significance between sexes. Significance determined via Welch's t test. Mean (SD) are shown. Black or red bars indicate normo- or hypertensive groups, respectively. n=60–200 human blood samples.

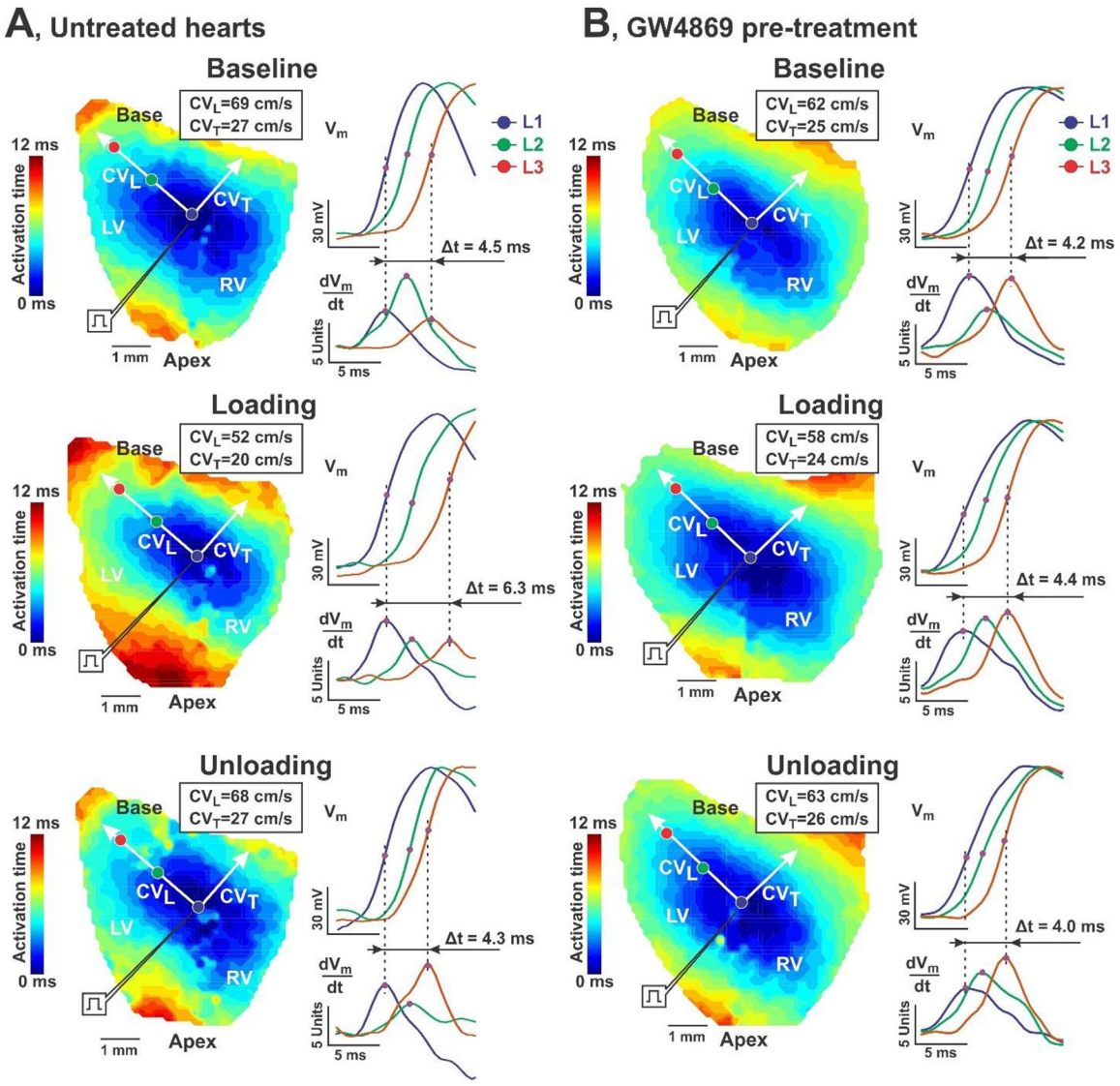

Fig. 8: Effect of stretch on ventricular conduction measured by fluorescence optical mapping in isolated mouse left ventricles.

Representative ventricular epicardial activation maps are shown for control hearts **(A)** and for hearts pre-treated with GW4869 (30 min prior loading) **(B)** before loading (baseline), after 10 min of loading (30 mmHg), and after 20 min of unloading. Activation maps were reconstructed during constant electrical pacing (8 Hz). Epicardial pacing at the center of the left ventricle produced an ellipsoidal spread of propagation with fast conduction parallel to the fiber axis (longitudinal conduction) and slow conduction perpendicular to the fiber axis (transverse conduction). Arrows show the directions of conduction velocity measurements longitudinal (CV_L) and transversal (CV_T). All the maps are plotted within the same time scale for comparison. The values of corresponding CVs are presented at the right upper corner of each map. Near the maps, superimposed upstrokes of optical action potentials (V_m) and their derivatives (dV/dt) corresponding to recording sites in longitudinal direction (L1, L2, and L3 circles in corresponding maps) are shown. Time delays (Δt) are shown for each condition. LV and RV – left and right ventricles.

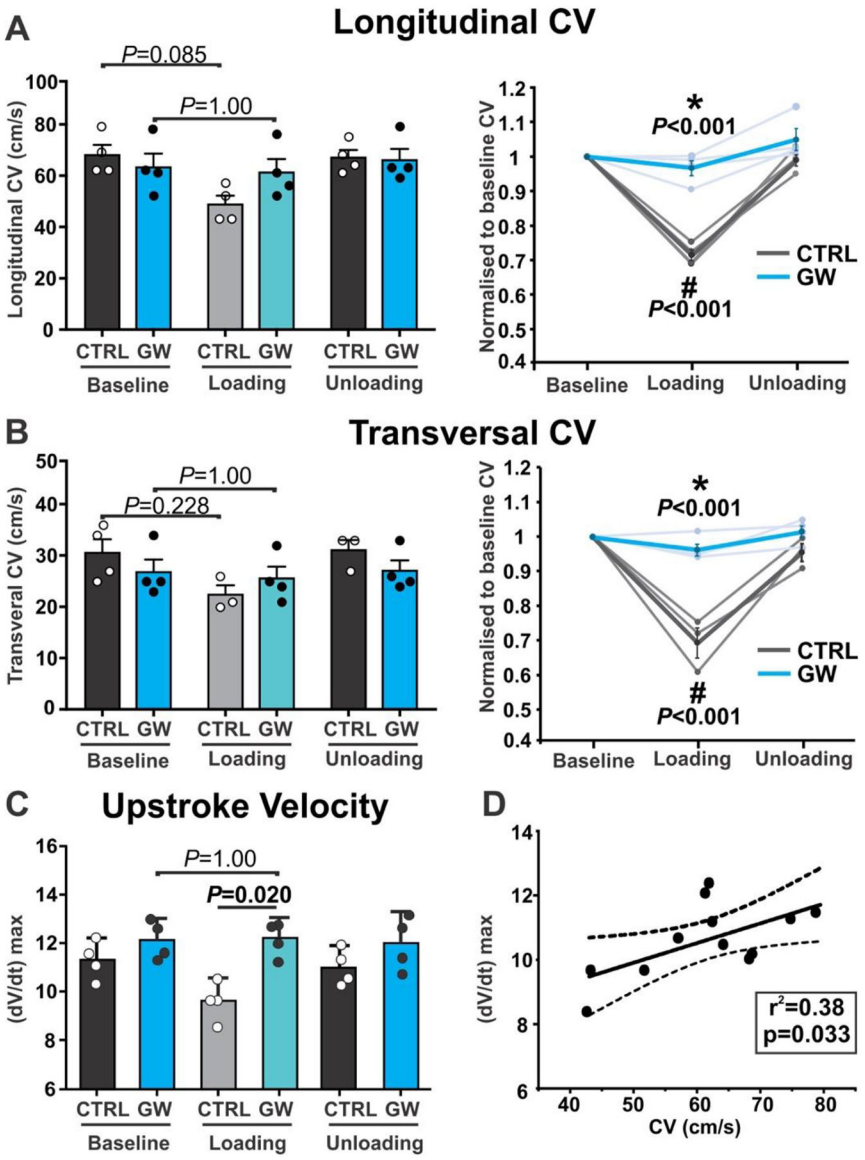

Fig. 9: Acute stretch reduces ventricular conduction and upstroke velocity via nSMase.

Mouse left ventricle longitudinal (**A**) and transversal (**B**) conduction velocity (CV) with normalization to baseline. Maximum upstroke velocity ($(dV/dt)_{max}$, **C**) and correlation between CV and maximum upstroke velocity (**D**) of mouse left ventricles (non-GW4869 treated only). CTRL – no treatment control, GW – GW4869 pre-treated. Significance determined via two-way ANOVA with *post-hoc* Bonferroni. Asterisks indicates significance between pre-treatment (GW4869 vs vehicle); # indicates significance between pressure loading conditions. Mean (SD) are shown, n=3–4 mice/group.